Supporting Information for

Drivers of improved $PM_{2.5}$ air quality in China from 2013 to 2017

Qiang Zhang[a,1,2], Yixuan Zheng[a,1], Dan Tong[a,b,1], Min Shao[c], Shuxiao Wang[b], Yuanhang Zhang[c], Xiangde Xu[d], Jinnan Wang[e], Hong He[f], Wenqing Liu[g], Yihui Ding[h], Yu Lei[e], Junhua Li[b], Zifa Wang[i], Xiaoye Zhang[d], Yuesi Wang[i], Jing Cheng[a], Yang Liu[a], Liu Yan[a], Qinren Shi[b], Guannan Geng[b], Chaopeng Hong[a], Meng Li[a], Fei Liu[b], Bo Zheng[b], Junji Cao[j], Aijun Ding[k], Jian Gao[l], Qingyan Fu[m], Juntao Huo[m], Baoxian Liu[b,n], Zirui Liu[i], Fumo Yang[o], Kebin He[b,2], and Jiming Hao[b,2]

[a] Department of Earth System Science, Tsinghua University, 100084 Beijing, China
[b] State Key Joint Laboratory of Environment Simulation and Pollution Control, School of Environment, Tsinghua University, 100084 Beijing, China
[c] College of Environmental Sciences and Engineering, Peking University, 100871 Beijing, China
[d] Chinese Academy of Meteorological Sciences, China Meteorological Administration, 100081 Beijing, China
[e] Chinese Academy for Environmental Planning, 100012 Beijing, China
[f] Research Center for Eco-Environmental Sciences, Chinese Academy of Sciences, 100085 Beijing, China
[g] Anhui Institute of Optics and Fine Mechanics, Chinese Academy of Sciences, 230031 Hefei, China
[h] National Climate Center, China Meteorological Administration, 100081 Beijing , China
[i] Institute of Atmospheric Physics, Chinese Academy of Sciences, 100029 Beijing, China
[j] Key Laboratory of Aerosol Chemistry and Physics, Institute of Earth Environment, Chinese Academy of Sciences, 710061 Xi'an, China
[k] School of Atmospheric Sciences, Nanjing University, 210023 Nanjing, China
[l] Chinese Research Academy of Environmental Sciences, 100012 Beijing, China
[m] Shanghai Environmental Monitoring Center, 200030 Shanghai, China
[n] Beijing Key Laboratory of Airborne Particulate Matter Monitoring Technology, Beijing Municipal Environmental Monitoring Center, 100048 Beijing, China
[o] Department of Environmental Science and Engineering, College of Architecture and Environment, Sichuan University, 610065 Chengdu, China

[1]Q.Z., Y. Zheng, and D.T. contributed equally to this work.

[2]To whom correspondence may be addressed. Email: qiangzhang@tsinghua.edu.cn, hekb@tsinghua.edu.cn, and hjm-den@tsinghua.edu.cn.

www.pnas.org/cgi/doi/10.1073/pnas.1907956116

Section S1 Clean air actions in China from 2013 to 2017

In support of the "Action Plan", a series of stringent clean air actions was implemented by China's central and local governments. Here we summarized six major measures implemented from 2013 to 2017. A brief description of the six measures was summarized in Fig. 1.

(1) *Strengthen industrial emission standards (IndEOP)*. Tighter emission standards along with stricter emission control measures were applied to thermal power plants and all emission-intensive industry sectors (e.g., iron and steel industry, cement industry) in China from 2013 to 2017. In 2012, the Chinese central government enforced the revised emission standard for thermal power plants (GB 13223-2011), whose emission limits were fully met by the end of 2015. To further reduce emissions from power sectors, the Chinese government enacted the "ultralow emission" standard for coal-fired power plants, which requests the emission limits for SO_2, NO_x, and particulates to be 35, 50, and 10 mg/m^3, respectively. By the end of 2017, 700 GW coal-fired power generation capacity were updated to meet the "ultralow emission" standard. As a result, 71% of national coal-fired power generation capacity and all power plants in the BTH regions operated at "ultralow emission" levels (1). Tighter emission standard for major industrial sectors were also enforced including standards for sintering and pelletizing of iron and steel industry (GB 28662-2012), iron smelt (GB 28663-2012), steel smelt (GB 28664-2012), steel rolling (GB 28665-2012), boiler (GB

13271-2014), flat glass (GB 26453-2011), brick (GB 29620-2013), and cement (GB 4915-2013). Take the cement industry as an example, emission limits of SO_2, NO_x, and particles from cement kiln reduced from 400, 800, and 100 mg/m^3, respectively, in the 2004 standard to 200, 400, and 30 mg/m^3, respectively, in the 2013 standard.

(2) *Phase out small and polluting factories (SmallInd)*. It is not only uneconomical but also infeasible to request small, scattered, and polluting enterprises to attain stringent emission standards by installing high-performance end-of-pipe control devices, which leads to the forced phasing out of these enterprises started from 2016, with a focus on the BTH and its surrounding regions. From 2016-2017, around 62,000 small and polluting enterprises in BTH and surrounding regions were phased-out or upgraded.

(3) *Phase out outdated industrial capacity (IndStru)*. In addition to the tighter emission standards in emission-intensive industries, outdated or inefficient technologies and capacity in various industry sectors were gradually phased out from 2013 to 2017. For example, 200 million tons of iron and steel production capacity, 250 million tons of cement production capacity, and 110 million weight boxes of flat glass production capacity were eliminated due to outdated technologies or overcapacity. Inefficient small power generation units were also retired to improve energy efficiency (i.e., 25 GW coal-fired power generation capacity were phased-out). As a consequence, the national average efficiency of coal-fired power plants, or grams of coal equivalent

consumed per kilowatt-hour of power supply, reduced from 321 gce kWh^{-1} to 309 gce kWh^{-1} from 2013 to 2017 (1).

(4) *Upgrades on industrial boilers (IndBoilder)*. As a major source of air pollutants, great attention was paid to coal-fired industrial boilers with actions of either eliminating small and inefficient boilers or applied stringent emission control to larger boilers. Nationally, more than 200,000 small coal boilers were shut down from 2013 to 2017. Existing and newly built large boilers were all equipped with SO_2 and particulate control devices as required by the new emission standard (GB 13271-2014).

(5) *Promote clean fuels in the residential sector (ResiCoal)*. Replacing coal in rural households with electricity and natural gas is the major action that targets the residential sector. Financial supports were provided and necessary infrastructures were constructed to ensure the implementation of this measure. By the end of 2017, energy consumption in 6 million households in China (4.8 million households in BTH and surrounding regions) switched from coal to electricity and natural gas.

(6) *Strengthen vehicle emission standards (CarCtrl)*. The "China 5" emission standard was applied to light gasoline and diesel vehicles in 2017, and oil quality was upgraded to be consistent with the emission standards. More than 20 million old and "yellow-label" vehicles (i.e., gasoline and diesel vehicles that fail to meet "China 1" and "China 3" standards) were eliminated from 2013 to 2017 and more than 1.7 million electric vehicles were introduced in stock.

Section S2 WRF-CMAQ modeling system

In this study, we applied the Weather Research and Forecasting model (WRF) version v3.5.1 (http://www.wrf-model.org/) and the Models-3 community multi-scale air quality (CMAQ) model version 5.1 to simulate the $PM_{2.5}$ concentrations over China. The WRF and CMAQ models in this study were configured following Zheng et al. (2015) (2). Meteorological parameters and concentration of air pollutants over China were simulated with a horizontal resolution of 36km×36km. Initial and boundary conditions (ICs and BCs) obtained from the National Centers for Environmental Prediction Final Analysis (NCEP-FNL) reanalysis data were applied to drive the WRF model. The CMAQ model was configured with CB05 as the gas-phase mechanism, AERO6 as the aerosol module, and Regional Acid Deposition Model (RADM) as the aqueous-phase chemistry model. Boundary conditions for the CMAQ simulations were provided by dynamic GEOS-Chem simulation (3). To ensure the continuity of model estimation, we conducted continuous CMAQ simulations for all scenario groups (in Table S1). For the continuous baseline simulations started from 2013, a one-month spin-up was applied (i.e., December of 2012), and initial conditions for the rest simulations were obtained from the *BASE* simulation (i.e., the first hour of each year).

Anthropogenic emissions for all scenarios (Table S1) over mainland China were processed by the Multi-resolution Emission Inventory of China (MEIC) (1, 4). Beyond mainland China, the anthropogenic emissions were derived from the MIX Asian emission inventory of 2010 (5). In addition to anthropogenic emissions, emissions from

other sources are required by CMAQ. In this case, biogenic emissions were calculated by Model of Emissions of Gases and Aerosols from Nature version 2.1 (MEGAN v 2.1) (6), which were driven by real-time meteorological conditions provided by our WRF simulations. Sea-salt and dust emissions were calculated online in the CMAQ model based on the algorithm developed by Gong (7) and a physical-based dust emission algorithm FENGSHA (8), respectively.

The WRF-CMAQ modeling system was utilized to simulate baseline $PM_{2.5}$ concentrations in China for the year 2013-2017 (i.e., *BASE* scenario group in Table S1) with anthropogenic emissions for mainland China obtained from Zheng et al. (2018) (1) and processed by the MEIC model (4). Variation of $PM_{2.5}$ concentrations from 2013 to 2017 over China and the three key regions were then estimated based on the *BASE* scenario group.

Section S3 Evaluation of simulated meteorological parameters

Meteorological parameters simulated by the WRF model were validated against ground-level observations that were collected from the National Climate Data Center (NCDC) (ftp://ftp.ncdc.noaa.gov/pub/data/noaa/). As presented in Table S7, the WRF model well predicted the domain-wide near-surface temperature and relative humidity with high R values and low mean biases. The WRF model slightly overestimated surface wind speed and precipitation, which might account for the underestimation of $PM_{2.5}$ concentrations. According to criteria provided by previous studies (9), the

validation results indicate that the WRF model provides acceptable performance in simulating meteorological parameters for further air quality simulations.

Through the *FixEmis* scenario, we tried to quantify the contribution of interannual meteorological variations to the 2013-2017 $PM_{2.5}$. Previous studies reveal that surface temperature, surface relative humidity, surface wind speed, and precipitation, which significantly affect formation, dispersion, and scavenging of aerosols, are important meteorological factors that drive variations in $PM_{2.5}$ concentrations (10-13). Therefore, the capability of the WRF model in accurately simulating interannual variations in these meteorological parameters is critical to the accuracy of simulated meteorologically driven interannual $PM_{2.5}$ variations (the *FixEmis* scenario group). Figs. S19-22 illustrate the observed and simulated monthly anomalies of the four major meteorological parameters relative to their 2013–2017 means for individual months in China and the three key regions (i.e., BTH, YRD, and PRD). The WRF model accurately captured the interannual monthly anomalies of temperature and relative humidity on the national scale and over the three key regions, with correlation coefficients (R) larger than 0.87. Simulated monthly anomalies of surface wind speed also correlated well with observations nationally and over BTH and YRD with R values around or larger than 0.85. Model performance in capturing interannual trends of precipitation was better in China (R=0.84) and YRD (R=0.74) than in BTH (R=0.62) and PRD (R=0.48). WRF performed better in predicting interannual trends of temperature and relative humidity than wind speed and precipitation, which is

consistent with annual validation results, as documented in Table S7. Generally, the WRF model well reproduced the interannual variations in meteorological parameters from 2013 to 2017, which supported the credibility of simulated meteorologically driven interannual variations in $PM_{2.5}$.

Section S4 Evaluation of simulated $PM_{2.5}$ concentration and chemical composition

Ground-level $PM_{2.5}$ observations from the national monitoring networks established and operated by China National Environmental Monitoring Center (http://beijingair.sinaapp.com) were used to evaluate the performance of our baseline CMAQ simulations of the years 2013-2017. Figs. S2 (a)-(e) compare simulated annual mean $PM_{2.5}$ concentrations with surface observations over the 74 cities which have continuous observations during 2013-2017. As shown in Fig. S2 (a)-(e), our model well reproduced the spatial distribution of $PM_{2.5}$ concentration across China with root mean square errors (RMSE) varied from 15.3 to 19.9 $\mu g/m^3$ for different years. Fig. S2 (f) presents the correlation coefficient between simulated daily $PM_{2.5}$ concentration and surface observations during 2013-2017. Of the 74 cities compared, 67 cities obtained correlation coefficient (R) higher than 0.6, indicating that our simulation can capture the variations of $PM_{2.5}$ concentration at the city level. Table S3 summaries the model performance statistics of daily $PM_{2.5}$ concentration over different regions during 2013-2017. CMAQ model generally performed well with R values ranging from 0.59 to 0.80

and normalized mean bias (NMB) from -17.2% to 17.1% over different years and regions.

As shown in Fig. S3 and S4, our model well reproduced interannual and monthly variations of $PM_{2.5}$ concentration for the three megalopolises over the modeling period, indicating that our model has the capability to capture the decreasing trend of $PM_{2.5}$ concentration from 2013 to 2017 for different regions. In summary, observed annual mean $PM_{2.5}$ concentration from 74 cities over China decreased from 69.8 $\mu g/m^3$ in 2013 to 47.0 $\mu g/m^3$ in 2017, respectively, while corresponding mean $PM_{2.5}$ simulations decreased from 67.4 $\mu g/m^3$ to 47.2 $\mu g/m^3$, respectively. Observed and simulated annual mean $PM_{2.5}$ declined by 33% and 30% from 2013 to 2017, respectively, indicating the consistent $PM_{2.5}$ reduction ratios in both observations and simulations.

We also evaluated modeled $PM_{2.5}$ chemical composition with observation data collected from various sources (Table S2). Compared to total $PM_{2.5}$ concentration, observations on $PM_{2.5}$ chemical composition are sparse in time and locations. We only selected observations with more than one-month data available and sampled simulated concentration with the locations and periods of observations. A total of 1501 observation data samples were collected for the major $PM_{2.5}$ chemical compositions, including sulfate (SO_4^{2-}), nitrate (NO_3^-), ammonium (NH_4^+), organic carbon (OC), and black carbon (BC). Locations, sample numbers, periods of observation, data frequency, as well as data sources are listed in Table S2, and locations of the observation sites are presented as triangles in Fig. S1.

Fig. S5 compares the modeled $PM_{2.5}$ chemical composition with ground measurement data collected in this study. In general, we found reasonable agreement between modeled and in-situ measured $PM_{2.5}$ chemical composition, with R values ranging from 0.65-0.75 for different species. The model performed well for NO_3^- and NH_4^+, while substantially overestimated BC concentration (NMB 40.8%) and underestimated SO_4^{2-} and OC concentration (NMB -32.1% and -28.5% respectively). Uncertainties in bottom-up emission inventories could be a plausible explanation for the discrepancies between model simulation and observations, specifically given that uncertainties in BC emission inventory are larger compared to other species (14). As most observation sites are located in urban areas, allocating too much BC emissions to urban areas when using the population as spatial proxy might be a particular reason for the overestimation of BC emissions (15). Underestimation of SO_4^{2-} and OC concentrations could also be partly attributed to the lack of model capability in simulating the heterogeneous formation of sulfate and secondary organic aerosols, respectively (2).

Section S5 Quantification of anthropogenic and natural drivers of $PM_{2.5}$ variations

To quantify the impacts of interannual variations in meteorological conditions and emission abatements on $PM_{2.5}$ levels, a *FixEmis* scenario (Table S1) with China's anthropogenic emissions of year the 2017 and varying meteorological conditions of the year 2013-2016 (including chemical boundary conditions) was conducted in addition

to the *BASE* simulations. The *FixEmis* provides the possible $PM_{2.5}$ levels in 2017 under the meteorological conditions of 2013-2016, and with additional information from *BASE*-2017 (i.e., baseline simulation for the year 2017), year-by-year impacts of meteorological variations from 2013 to 2017 (i.e., meteorology-related $PM_{2.5}$ variations) can be derived. Emission-related $PM_{2.5}$ variations can also be derived by interannual $PM_{2.5}$ variations obtained from *BASE* less corresponding meteorology-related $PM_{2.5}$ variations.

Section S6 Evaluation of simulated meteorologically driven $PM_{2.5}$ variations

Ground-level $PM_{2.5}$ observations were applied to evaluate the interannual meteorologically-driven variations in $PM_{2.5}$ concentrations as simulated by the *FixEmis* scenario. Similar to the evaluation for baseline simulation, observations from monitoring sites operated continuously through 2013-2017 over 74 key cities were utilized here.

National or regional monthly mean $PM_{2.5}$ observations and the corresponding simulations were first obtained. Monthly mean $PM_{2.5}$ observations were then detrended by removing trends derived from a linear regression model to exclude the impacts of anthropogenic emission control. Monthly anomalies of detrended observations and *FixEmis* simulations relative to their 2013–2017 means for individual months were further calculated to reflect the meteorologically-driven interannual variations in $PM_{2.5}$ concentrations (Fig. S11). The correlation coefficients (R) between anomalies of

detrended observations and *FixEmis* simulations range from 0.77 to 0.84 across regions, which indicates good consistency between observations and simulations over all regions. This result implies the capability of our *FixEmis* simulations in well capturing the meteorologically-driven interannual $PM_{2.5}$ variations in all study regions.

Section S7 Estimation of occurrence frequency of air stagnation days

We applied the approach developed by Wang et al. (2018) (16) to estimate the occurrence frequency of stagnation days from 2013 to 2017. This approach considers the capability of atmospheric horizontal dispersion, the strength of atmospheric mixing, and wet deposition. It uses surface wind speed (Wsp), boundary layer height (PBLH), and occurrence of precipitation as indicators.

We retrieved hourly wind components at 10 m (parameters: U10M, V10M), planetary boundary layer height (parameter: PBLH), and total precipitation (parameter: PRECTOT) at a spatial resolution of 0.5° × 0.625° from the Modern-Era Retrospective analysis for Research and Applications, Version 2 (MERRA-2) dataset. Wind speed at 10m was calculated based on U and V wind components at 10 m.

Fitted models that describe the seasonal dependence of normalized daily $PM_{2.5}$ concentrations on the 10-m wind speed and boundary layer height in Wang et al. (2018) (16) were applied. Fitted models for four seasons are listed as Eqs. (S1)-(S4) for spring, summer, autumn, and winter, respectively.

$$PBLH = 3.57 \times 10^3 \times e^{-3.35 \times Wsp} + 0.352 \quad \text{(S1)}$$

$$PBLH = 7.66 \times 10 \times e^{-2.12 \times Wsp} + 0.443 \quad \text{(S2)}$$

$$PBLH = 1.88 \times 10^4 \times e^{-5.15 \times Wsp} + 0.440 \quad \text{(S3)}$$

$$PBLH = 0.759 \times 10^3 \times e^{-0.6 \times Wsp} + 0.264 \quad \text{(S4)}$$

An air stagnation day is identified when no precipitation occurs over the day and the daily PBLH retrieved from the MERRA-2 dataset is less than the modeled PBLH threshold from Eqs. (S1)-(S4). National and regional monthly mean population-weighted occurrence frequencies of air stagnation were then derived.

We applied the derived occurrence of air stagnation days and ground-based $PM_{2.5}$ observations to test the impacts of air stagnation conditions on $PM_{2.5}$ concentrations. We found that national annual mean $PM_{2.5}$ observations in air stagnation days were higher than that in non-stagnation days by 35% to 52% from 2013 to 2017, which confirms that air stagnation conditions would exacerbate $PM_{2.5}$ pollutions.

Section S8 Measure-by-measure estimation of emission abatements

In this study, we conducted a measure-by-measure evaluation to quantify the benefits of the "Action Plan". According to the "Action Plan", six major measures implemented over 2013-2017 were summarized, as listed in Fig. 1 and Section S1. Emission reductions in 2017 from the five-year implementation of each control measure were then estimated.

The bottom-up emission inventory for 2013-2017 was obtained from the MEIC model (1) as the baseline of the emission estimates. To quantify the emission reductions in 2017 from the implementation of the "Action Plan", we introduced a series of "uncontrolled" scenarios for each of the six emission control measures in 2017 that assumed those measures had not taken effect from 2013 to 2017 and that changes in the activity rates, energy efficiencies, technology distributions, and penetrations of end-of-pipe (EOP) control measures linked to those measures did not occur before 2013. Emissions of each "uncontrolled" scenario were then estimated by implementing those assumptions into the MEIC model framework, and the 2017 emission reductions of each measure were quantified as the differences between the "uncontrolled" scenario emissions and baseline emissions.

Specifically, the emission reductions of each control measure ($\Delta Emis$) were estimated as:

$$\Delta Emis_{m,k} = \sum_{j}\left(A'_{j} \times \sum_{i}\left(X'_{i,j} \times EF_{i,j,k} \times \sum_{n}\left(C'_{i,j,n} \times \left(1-\eta_{k,n}\right)\right)\right)\right) - \sum_{j} EmisReal_{\mathrm{j}} \quad \text{(S5)}$$

where m represents the control measures defined in this study, k represents air pollutants, j represents emission sources related to measure m, i represents technologies of combustion or production, n represents air pollution control technologies, A' is the estimated activity rate under the "uncontrolled" scenario, X' is the estimated penetration of a specific combustion or production technology under the "uncontrolled" scenario, EF is the unabated emission factor, C' is the estimated

penetration of a specific pollution control technology under the "uncontrolled" scenario, η is the removal efficiency of a given control technology, and $EmisReal$ represents baseline emissions in 2017, which were obtained from MEIC (1). Detailed methods for quantifying the activity rates (*A'*), technology distribution (*X'*), and penetration of control technologies (*C'*) of each of the six "uncontrolled" scenarios are documented below.

(1) Strengthen industrial emission standards.

As documented in Section S1, this measure aims to install advanced pollution control equipment in power plants, iron and steel production, cement production, and flat glass production by the implementation of new emission standards in these sectors from 2013 to 2017 (see Table S6). By implementing the new standards, penetrations of advanced pollution control technologies in the abovementioned sectors (*C'* in Eq. (S5)) have been substantially increased from 2013 to 2017.

For the power sector, as of 2017, 71% of total operating coal-fired generating capacity (~700 GW) were upgraded with high-efficient emission control facilities to meet the so-called "ultralow" emission standard. Table S6 summaries the penetrations and removal efficiencies of different emission control facilities in China's power sector in 2017. Under the "uncontrolled" scenario, we assumed that no additional new standard supplemented after 2013. We therefore projected that from 2013 to 2017, the end-of-pipe control technologies and their operating conditions would retain at the level of the year 2013 or be upgraded to meet the requirement of power plant emission

standard (17) published in 2012. The estimated penetrations and removal efficiencies of emission control technologies in power plants in 2017 under the "uncontrolled" scenario are also listed in Table S6.

Similarly, emission abatements from strengthening end-of-pipe emission standards in iron and steel, cement, and flat glass manufacturing industries were all estimated following the same approach as that applied to the power sector. Table S6 summaries the penetrations of different emission control technologies in the abovementioned sectors in 2017 under the baseline emission inventory and the "uncontrolled" scenario.

(2) Phase out small and polluting factories.

Driven by the tightened emission standards, this measure aims at small and polluting factories to be replaced by large facilities with clean production technologies and advanced pollution control equipment. By phasing out small and polluting factories, penetrations of outdated production technologies (X' in Eq. (S5)) and penetrations of low-efficiency pollution control technologies in industrial sectors (C' in Eq. (S5)) have been substantially decreased from 2013 to 2017 as to replace these factories with large and clean facilities that meet emission standards.

From 2016-2017, more than 62,000 small and polluting enterprises in BTH and surrounding regions were renovated, which are mainly scattered in various non-key industrial sectors. Table S6 summaries the penetrations of outdated production technologies and low-efficient end-of-pipe control technologies in 2017 in related industrial sectors. Under the "uncontrolled" scenario, we projected that the penetrations

of production technologies and the penetrations of emission control technologies in related industrial sectors would remain unchanged from 2013 to 2017 when assuming that no additional new policy targeted small and polluting factories after 2013. We used the enterprise-level database (18), which includes the basic information of each small and polluting enterprise (e.g., location, production capacity, and production technology). On this basis, we summarized the proportions of these small and polluting enterprises, the corresponding penetrations of different production technologies and end-of-pipe control technologies in each industrial sector. Table S6 also lists the estimated parameters in China's non-key industrial sectors in 2017 under the "uncontrolled" scenario.

(3) Phase out outdated industrial capacity.

Phasing out outdated or inefficient technologies and capacity in power and industrial sectors is carried out by the implementation of new efficiency, environment, and safety standards from 2013 to 2017 (see Table S6). The average energy intensity or energy consumed per unit of industrial gross output gradually decreased by eliminating outdated or inefficient technologies and capacities. As a consequence, part of energy consumptions (A' in Eq. (S5)) in power and industrial sectors has been saved when generating the same amount of electricity or producing the same amount of industrial products due to the improvement of energy efficiency.

For the power sector, in total, more than 25 GW coal-fired power generating capacity were phased out during the period 2013-2017. As a result, the average

efficiency of coal-fired power generating units has been significantly improved by 4% (see Table S6). Without this measure, we projected that only moderate improvement of 2% in energy efficiency had been achieved according to "12th Five-Year-Plan (2011-2015)" (19) under the "uncontrolled" scenario.

Same with the approach applied to the power sector, we assumed that the energy consumed per unit of industrial gross output in iron and steel production, cement production, and flat glass production would stay at the level of the year 2013. The activity rates from the MEIC model and the estimated activity rates under the "uncontrolled" scenario in the abovementioned sectors are all listed in Table S6.

(4) Upgrades on industrial boilers.

Emission reductions from upgrades on industrial boilers includes not only eliminating small and inefficient coal-fired boilers but also installing advanced pollution control equipment on larger boilers by the implementation of new emission standards from 2013 to 2017 (see Table S6). The average energy intensity has been greatly decreased by eliminating small and inefficient boilers. As a result, energy consumptions (*A'* in Eq. (S5)) in industrial boilers have been partially saved and emissions of CO_2 and air pollutants have been substantially reduced. Meanwhile, by implementing the new emission standards, penetrations of advanced pollution control technologies in industrial boilers (*C'* in Eq. (S5)) has been gradually increased from 2013 to 2017.

On the one hand, as of 2017, more than 200,000 small coal-fired boilers (≤7 MW) were shut down from 2013 to 2017. Therefore the energy efficiency of coal-fired boilers has been greatly improved. On the other hand, more than half of the total operating coal-fired boilers' capacity was upgraded with high-efficient SO_2 and PM emission control facilities to meet the new emission standard (20) (see Table S6). In this case, we assumed that no additional new standard issued after 2013 and projected that the end-of-pipe control technologies and their operating conditions by the end of 2017 under the "uncontrolled" scenario would be the same level as the year 2013. As summarized in Table S6, we therefore projected a larger coal consumption in industrial boilers and lower penetration rates of advanced control technologies installed in coal-fired industrial boilers in 2017 under the "uncontrolled" scenario.

(5) Promote clean fuels in the residential sector.

Actions are taken in the residential sector include decreasing the penetrations of direct coal-burning in the residential sector by replacing coal with natural gas and electricity; increasing the penetrations of clean coal use by switching from raw coal to clean coal briquettes with lower levels of sulfur and ash contents; and reducing the average emission levels by increasing the penetrations of advanced and clean stoves from 2013 to 2017 (see Table S6). The energy structure and activity rates in the residential sector (A' in Eq. (S5)) have been changed from 2013 to 2017 by replacing coal with electricity and natural gas, as well as promoting clean coal use. And the

penetrations of advanced stoves in the residential sector (*X'* in Eq. (S5)) increase from 2013 to 2017 by replacing older stoves with advanced and clean stoves.

By the end of 2017, energy consumptions in six million households in China (4.8 million households in the BTH and surrounding regions) switched from coal to electricity and natural gas. Advanced and clean stoves have been widely promoted under the governments' financial supports. Meanwhile, the proportion of coal washing has been significantly increased to ~70% by 2017. Under the "uncontrolled" scenario, the assumption that there are no additional actions taken in the residential sector from 2013 to 2017 is applied, and we projected the same energy structure, the proportions of coal washing and penetrations of advanced stoves as those in 2013 under the "uncontrolled" scenario. Table S6 lists the parameters estimated in 2017 under both the baseline emission inventory and the "uncontrolled" scenario.

(6) Strengthen vehicle emission standards.

The reduction of emissions in the road transportation sector is mainly achieved through fleet turnover, which means that old vehicles were replaced by new and clean vehicles through the implementation of stringent vehicle emission standards. Penetrations of new emission standards for various vehicle types (*C'* in Eq. (S5)) have been substantially increased from 2013 to 2017 as a result of implemented new standards.

The "China 5" emission standard was implemented to light gasoline and diesel vehicles in 2017, and newly registered vehicles must comply with these stringent

emission standards. Additionally, more than 20 million old and "yellow-label" vehicles were eliminated from 2013 to 2017. Table S6 summaries the penetrations of different emission standards for various vehicle types in China's road transportation sector in 2017. Under the "uncontrolled" scenario, we assumed the "China 5" emission standard would be applied nationwide in 2018 as planned except some key cities (21). At the same time, "yellow label" vehicles wouldn't be thoroughly eliminated without compulsory phase-out measures from the "Action Plan". As projected in Table S6, the penetrations of vehicles that meet the "China 5" emission standard are pretty small in 2017 under the "uncontrolled" scenario.

Section S9 Evaluation of air quality benefits of emission control

Six simulations for the *MEAS* scenario group, as listed in Table S1, were conducted to quantify air quality improvements in 2017 as contributed by each measure. *MEAS* simulations were all driven by meteorological conditions and boundary conditions for the year 2017 as the same as of *BASE-2017*. For each *MEAS* simulation, emission reductions introduced by the corresponding control measure were added to the 2017 baseline emission and the derived emission inventory was then applied to drive the corresponding air quality modeling. Measure-specific $PM_{2.5}$ reductions were quantified as the difference between each corresponding simulation (e.g., *MEAS-IndEOP*, *MEAS-SmallInd*) and the *BASE-2017* simulation. To avoid the nonlinear relationship between emissions and modeled $PM_{2.5}$ concentrations, we added a *NoCtrl*

scenario, which represents a case that the six control measures were all unimplemented. Baseline emissions in 2017 and total emission reductions contributed by the six measures were added together to drive the air quality simulation of the *NoCtrl* scenario. Simulated measure-related $PM_{2.5}$ reductions were then normalized by the difference between the *NoCtrl* and *BASE-2017* scenarios.

Section S10 Quantification of avoided mortality related to emission control

Relationships between chronic exposure and attributable deaths, which are called C–R relationships, are necessary for evaluating the excess deaths attributable to $PM_{2.5}$ exposure. Previous studies majorly applied the integrated concentration-response functions (IER) developed for the Global Burden of Diseases Study (GBD) as the C-R relationships to calculate mortality (22-24). However, the IER functions provide C-R relationships at high $PM_{2.5}$ concentrations by incorporating information on $PM_{2.5}$–mortality associations from non-ambient $PM_{2.5}$ sources, including secondhand smoke, household air pollution from the use of solid fuels, and active smoking (24). These non-ambient $PM_{2.5}$-mortality associations in IER functions may bias estimated mortality over highly polluting regions like China.

To resolve the uncertainties introduced by non-ambient $PM_{2.5}$-mortality associations, Burnett et al. (2018) (25) recently built Global Exposure Mortality Model (GEMM), which provide C–R relationships for a wide range of ambient $PM_{2.5}$ distributions by incorporating cohort studies of ambient $PM_{2.5}$ exposure from both clean

(e.g., Europe and the North America) and polluting regions (e.g., China). The incorporation of a Chinese man cohort, which provides $PM_{2.5}$-mortality relationships observed at a high pollution level with long-term ambient $PM_{2.5}$ exposures up to 84 $\mu g/m^3$, greatly extending the range of exposures observed in cohort studies conducted in clean regions in Europe and North America. Higher confidence in $PM_{2.5}$-mortality relationships at high $PM_{2.5}$ levels makes GEMM more suitable for application in China. We therefore applied the newly developed GEMM model to calculate the premature mortality attributable to chronic $PM_{2.5}$ exposure in China (25).

The GEMM was built for estimating $PM_{2.5}$-related nonaccidental deaths due to noncommunicable diseases and LRIs (also denoted as GEMM NCD+LRI). To facilitate comparison with the IER model, Burnett et al. (2018) (25) also provide GEMM 5-COD model for mortality estimation based on the five separate causes considered in the IER model (i.e., lung cancer, chronic obstructive pulmonary disease, ischemic heart disease, cerebrovascular disease, and lower respiratory infections). In this study, we chose the GEMM NCD+LRI, which is the core model of GEMM (25), for our mortality estimation.

The GEMM NCD+LRI parameterizes the dependence of relative risk (RR) of NCD+LRI on concentration (C) (25):

$$RR(C) = e^{\frac{\theta \times \ln\left(\frac{z}{\alpha}+1\right)}{1+e^{\left(-\frac{z-\mu}{\nu}\right)}}}, \text{ where } z = \max(0, C - 2.4) \quad \text{(S6)}$$

θ, α, μ and ν are parameters that determine the shape of the concentration-response relationships. According to the parameters provided by the GEMM framework, RR of

NCD+LRI were calculated by age for adults with every 5-year interval from 25 to age larger than 85. Premature mortality for a population subgroup p (population by age and gender) in grid i were further calculated:

$$M_{p,i}(C_c) = P_{p,i} \cdot B_p \cdot \frac{RR_p(C_i)-1}{RR_p(C_i)} \quad \text{(S7)}$$

where $P_{p,i}$ is the population amount of a population subgroup in grid cell i, B_p represents the national average annual mortality incidence rate of NCD+LRI for a population subgroup, and $RR_p(C_i)$ is the relative risk of NCD+LRI for population subgroup p at $PM_{2.5}$ exposure level of C_i. National base mortality incidence and demographic information were both retrieved from the GBD2016 study (26). Gridded population distribution for 2015 with a horizontal resolution of 0.1°×0.1° was collected from the Global Population for the World (GPW) dataset (27) and scaled to the 2017 level based on population statistics from the National Bureau of Statistics of China. In this study, a distribution of 1,000 point estimates of θ calculated based on parameters provided by the GEMM NCD+LRI was utilized and propagated to calculate mean attributable mortality and its 95% confidential intervals (CI) (25).

Due to the availability of input data, $PM_{2.5}$-induced premature mortality was calculated on a horizontal resolution of 0.1°×0.1° based on national baseline mortality incidence and demographic information for 2016, scaled population distribution for 2017, and simulated $PM_{2.5}$ concentrations. The calculated mortality was rounded to the nearest hundred for presentation.

Because of the supralinear relationship between $PM_{2.5}$ concentration and its attributable mortality in the GEMM NCD+LRI framework, total avoided premature mortality from the implementation of the six major control measures were calculated as the difference between the *NoCtrl* and *BASE-2017* scenarios to avoid the nonlinear effect. We assumed that unit concentration reduction associated with each measure contributes equally to avoided premature mortality, and therefore, we attributed the avoided premature mortality to the implementation of each control measure on the provincial level by a direct proportion approach (28). On the provincial level, the proportion of avoided mortality from a measure is equivalent to the proportion of abated population-weighted annual mean $PM_{2.5}$ contributed by the measure. The calculated mortality was rounded to the nearest hundred for presentation.

Section S11 Quantification of mortality by other models

We also calculated $PM_{2.5}$ attributable premature mortality based on the GEMM 5-COD model and the IER model to test the changes in mortality estimated by different C-R models. The mortality calculation based on the GEMM 5-COD and IER models applied the same inputs as utilized to calculate mortality based on the GEMM NCD+LRI.

Five endpoints were considered for these two models, including lung cancer (LC), chronic obstructive pulmonary disease (COPD), ischemic heart disease (IHD), cerebrovascular disease (stroke), and lower respiratory infections (LRI). Different age

groups were selected for mortality estimations based on different models, according to Burnett et al. (2018) (25) and Cohen et al. (2017) (29). By applying the GEMM-5COD model, mortality induced by all the five endpoints was calculated for adults (25). While applying the IER model, mortality induced by the former four endpoints was calculated for adults and mortality induced by LRI was calculated for children under 5 (24). According to the functions provided by GEMM 5-COD and IER models, RR of IHD and stroke were calculated by age, and all-age RR were calculated for the other three endpoints.

GEMM 5-COD follows the same approach as documented in Section S10 to calculate $PM_{2.5}$-related mortality by applying parameters for each endpoint obtained from Burnett et al. (2018) (25). GEMM 5-COD also applies the same approach to calculate 95% CI of estimated mortality as used by GEMM NCD+LRI.

The IER functions parameterize the dependence of relative risk (RR) for each of the five endpoints on concentration (C) (24):

$$RR(C) = \begin{cases} 1 + \beta\left(1 - e^{-\gamma(C-C_0)^{\delta}}\right), if\ C > C_0 \\ 1 \qquad\qquad\qquad\qquad\quad , if\ C \leq C_0 \end{cases} \tag{S8}$$

where C_0 is the endpoint-specific theoretical minimum-risk exposure level of $PM_{2.5}$, below which, no health risks of $PM_{2.5}$ exposure is assumed; and β, γ, and δ are parameters that determine the shape of the concentration-response relationships. Mortality can further be estimated by applying IER-based RR derived from Eq. (S8) to Eq. (S7). A distribution of 1,000 point estimates of C_0, β, γ, and δ parameters

provided by the IER was utilized and propagated to calculate mean attributable mortality and its 95% CI (24).

Results of national and regional $PM_{2.5}$ attributable premature mortality in *BASE-2017* and *NoCtrl* scenarios estimated by GEMM NCD+LRI, GEMM 5-COD, and IER models are shown in Table S5.

Section S12 Uncertainty analysis

Our results were subject to a number of uncertainties and limitations. The uncertainty ranges (95% confidence interval) in different steps of our analysis are discussed below.

First, the $PM_{2.5}$ concentrations simulated by the air quality model were unavoidably affected by the inherent uncertainties of the emission inventories and the model representation of chemical and physical processes of the WRF-CMAQ model. The computational intensity of the WRF-CMAQ model makes it infeasible to estimate related uncertainties by conducting sensitivity simulations that require large numbers of computational resources. Instead, we used the normalized standard deviation (NSD) of the simulated $PM_{2.5}$ against the ground-based $PM_{2.5}$ observation to represent the overall model uncertainties for each province. The provincial relative error of the annual average $PM_{2.5}$ simulations was estimated for each individual year over 2013-2017. We assumed that all NSD of the simulated $PM_{2.5}$ concentrations were normally distributed and all grids within a province follow the same distribution. We also

assumed that the annual NSD of the simulated $PM_{2.5}$ concentrations derived from the *BASE* scenario applies to simulations that conducted in the corresponding years for all other scenarios (i.e., *FixEmis*, *MEAS*, *NoCtrl*). Uncertainties of annual $PM_{2.5}$ simulations, variations in simulated $PM_{2.5}$ concentrations, interannual meteorologically driven $PM_{2.5}$ variations, and measure-specific contributions to $PM_{2.5}$ variations were then estimated by 1,000 random samplings of $PM_{2.5}$ distributions for each scenario- and year-specific simulation based on the simulated $PM_{2.5}$ concentrations and the corresponding NSD.

Second, our mortality estimation was subject to uncertainty due to the limited epidemiology evidence in the GEMM functions. To consider the uncertainty introduced by the GEMM functions, a distribution of 1,000 point estimates of θ calculated based on parameters provided by the GEMM NCD+LRI was utilized and propagated to calculate mean attributable mortality and its 95% confidential intervals. For a given set of GEMM parameters, 1,000 random samplings of the normal distribution of $PM_{2.5}$ concentrations in each grid cell were provided as inputs to include the uncertainty associated with $PM_{2.5}$ concentrations.

List of Figures

Fig. S1 Study domain of the CMAQ model and the spatial distribution of monitoring sites used in this study. Grey circles depict site locations in the 74 major cities where $PM_{2.5}$ concentrations were measured continuously during 2013-2017. Red triangles depict locations of collected $PM_{2.5}$ chemical compositions observations, as summarized in Table S2. Multi-year observations of $PM_{2.5}$ chemical compositions were collected in Beijing, Tianjin, Nanjing, and Xi'an as depicted by blue triangles, where changes in $PM_{2.5}$ chemical compositions are illustrated in Fig. S17. Blue lines outline the three key regions, namely, the Beijing-Tianjin-Hebei region (BTH), the Yangtze River Delta region (YRD), and the Pearl River Delta region (YRD).

Fig. S2 Evaluation of simulated $PM_{2.5}$ concentration against surface $PM_{2.5}$ observations. (a)-(e) Spatial distributions of simulated annual mean $PM_{2.5}$ concentrations during 2013-2017. Measured annual mean $PM_{2.5}$ concentrations in 74 cities were overlayed. Statistics of annual mean $PM_{2.5}$ simulations against observations in 74 cities are provided. R, NMB, and RMSE stand for the correlation coefficient, normalized mean bias, and root mean squared error, respectively. (f) Simulated five-year mean $PM_{2.5}$ concentrations during 2013-2017. The correlation coefficient between simulated and observed daily mean $PM_{2.5}$ concentration during 2013-2017 was overlaid for each city.

Fig. S3 Regional-averaged annual mean $PM_{2.5}$ observations and simulations from 2013 to 2017 for (a) China, (b) BTH, (c) YRD, and (d) PRD. Simulations were sampled by observations spatially and temporally.

Fig. S4 Comparison between simulated and observed monthly mean $PM_{2.5}$ concentrations for (a) China, (b) BTH, (c) YRD, and (d) PRD from 2013 to 2017. Simulations were sampled with observations.

Fig. S5 Evaluation of simulated $PM_{2.5}$ chemical composition concentrations against ground-based observations. The solid line corresponds to the 1:1 line, and the dashed lines correspond to the 1:2 and 2:1 lines. R, NMB, and N stand for the correlation coefficient, normalized mean bias, and sample number, respectively.

Fig. S6 Spatial distribution of annual mean $PM_{2.5}$ concentrations in China for (a) 2014, (b) 2015, and (c) 2016.

Fig. S7 Sectoral emission of SO_2, NO_x, and $PM_{2.5}$ from 2013 to 2017 in (a) China, (b) BTH, (c) YRD, and (d) PRD.

Fig. S8 Annual population-weighted mean $PM_{2.5}$ concentrations in China and the three key regions from 2013 to 2017. Labels over bars depict reduction ratios of simulated $PM_{2.5}$ concentration for each region from 2013 to 2017.

Fig. S9 Changes in annual population-weighted mean $PM_{2.5}$ concentrations contributed by anthropogenic emission control (blue bars) and meteorological condition changes (yellow bars) between 2013 and 2017 for (a) China, (b) BTH, (c) YRD, and (d) PRD.

Fig. S10 Variations in monthly population-weighted mean $PM_{2.5}$ concentrations driven by varying meteorological conditions and fixed emissions in 2017 over 2013-2017 for (a) China, (b) BTH, (c) YRD, (d) PRD.

Fig. S11 Time series of monthly anomalies of detrended $PM_{2.5}$ observations and $PM_{2.5}$ concentrations simulated in the *FixEmis* scenario relative to their 2013–2017 means for individual months in China and the three key regions. (a) China, (b) BTH, (c) YRD, (d) PRD. Simulations were sampled with observations.

Fig. S12 Map of changes in annual mean $PM_{2.5}$ concentrations induced by interannual variations in meteorological conditions between 2013 and 2017.

Fig. S13 Emission reductions in SO_2, NO_x, and $PM_{2.5}$ obtained in 2017 contributed by the five-year implementation of the six clean air measures (unit: 10^4 ton) over China and the three key regions. The tick labels on the y-axis depict the fraction of emission reductions contributed by each measure out of the total emission.

Fig. S14 Contribution of $PM_{2.5}$ abatements from the six control measures for (a) China, (b) BTH, (c) YRD, and (d) PRD.

Fig. S15 Avoided $PM_{2.5}$-attributable premature mortalities from the six clean air measures at a national scale and over the three key regions. Labels depict the avoided excess deaths introduced by the individual measure.

Fig. S16 Comparison of emission trends, model simulation trends, and observation trends from both ground and space for SO_2 (red lines) and NO_2 (blue lines) during 2013-2017 over Eastern China. Solid lines, dashed lines, dash-dot lines, and dotted lines represent emissions, ground observations, model simulations, and satellite vertical column densities from OMI, respectively. Eastern China here includes the provinces of Beijing, Tianjin, Hebei, Shanxi, Shaanxi, Shandong, Henan, Hubei, Anhui, Jiangsu, Shanghai, and Zhejiang.

Fig. S17 Comparison of simulated and observed concentration changes in $PM_{2.5}$ chemical compositions in Beijing, Tianjin, Nanjing, and Xi'an. Information on observation sites is presented in Table S2. Values over bars show the percentage decreases in $PM_{2.5}$ chemical compositions during the two periods as defined for each city.

Fig. S18 Methodology framework for this study. This framework consists of two parts: an evaluation of $PM_{2.5}$ variation and anthropogenic and meteorological drivers of $PM_{2.5}$ variations from 2013 to 2017 (left panel) and estimation of the benefits of each emission control measure (right panel). The WRF model, CMAQ model, MEIC model, and GEMM functions represent the Weather Research and Forecasting Model, Community Multiscale Air Quality Model, the Multi-resolution Emission Inventory for China, and the Global Exposure Mortality Model, respectively.

Fig. S19 Time series of monthly anomalies of four major meteorological parameters relative to their 2013–2017 means for individual months in China. (a) Temperature, (b) relative humidity, (c) surface wind speed, (d) daily precipitation. Simulations were sampled with observations.

Fig. S20 Time series of monthly anomalies of four major meteorological parameters relative to their 2013–2017 means for individual months in the BTH region. (a) Temperature, (b) relative humidity, (c) surface wind speed, (d) daily precipitation. Simulations were sampled with observations.

Fig. S21 Time series of monthly anomalies of four major meteorological parameters relative to their 2013–2017 means for individual months in the YRD region. (a) Temperature, (b) relative humidity, (c) surface wind speed, (d) daily precipitation. Simulations were sampled with observations.

Fig. S22 Time series of monthly anomalies of four major meteorological parameters relative to their 2013–2017 means for individual months in the PRD region. (a) Temperature, (b) relative humidity, (c) surface wind speed, (d) daily precipitation. Simulations were sampled with observations.

Fig. S1.

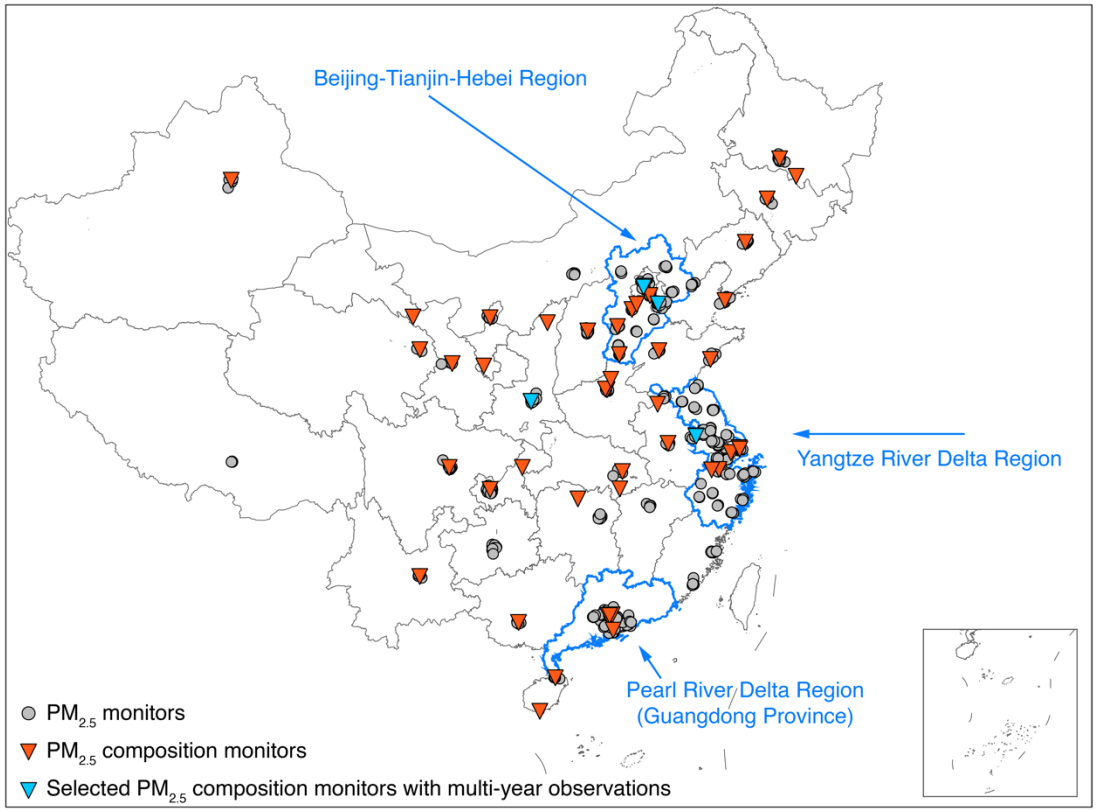

Fig. S1 Study domain of the CMAQ model and the spatial distribution of monitoring sites used in this study. Grey circles depict site locations in the 74 major cities where $PM_{2.5}$ concentrations were measured continuously during 2013-2017. Red triangles depict locations of collected $PM_{2.5}$ chemical compositions observations, as summarized in Table S2. Multi-year observations of $PM_{2.5}$ chemical compositions were collected in Beijing, Tianjin, Nanjing, and Xi'an as depicted by blue triangles, where changes in $PM_{2.5}$ chemical compositions are illustrated in Fig. S17. Blue lines outline the three key regions, namely, the Beijing-Tianjin-Hebei region (BTH), the Yangtze River Delta region (YRD), and the Pearl River Delta region (YRD).

Fig. S2.

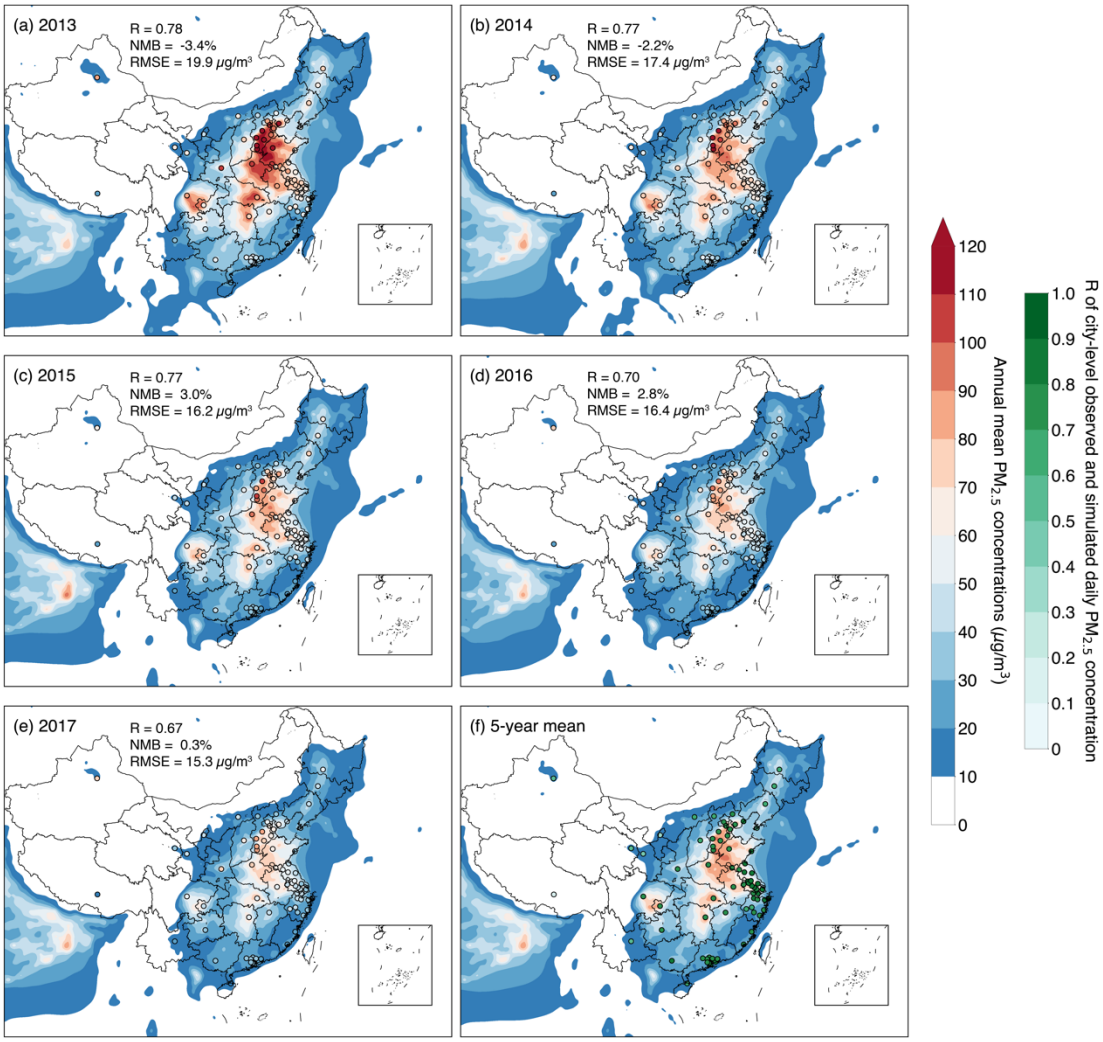

Fig. S2 Evaluation of simulated $PM_{2.5}$ concentration against surface $PM_{2.5}$ observations. (a)-(e) Spatial distributions of simulated annual mean $PM_{2.5}$ concentrations during 2013-2017. Measured annual mean $PM_{2.5}$ concentrations in 74 cities were overlayed. Statistics of annual mean $PM_{2.5}$ simulations against observations in 74 cities are provided. R, NMB, and RMSE stand for the correlation coefficient, normalized mean bias, and root mean squared error, respectively. (f) Simulated five-year mean $PM_{2.5}$ concentrations during 2013-2017. The correlation coefficient between simulated and observed daily mean $PM_{2.5}$ concentration during 2013-2017 was overlaid for each city.

Fig. S3.

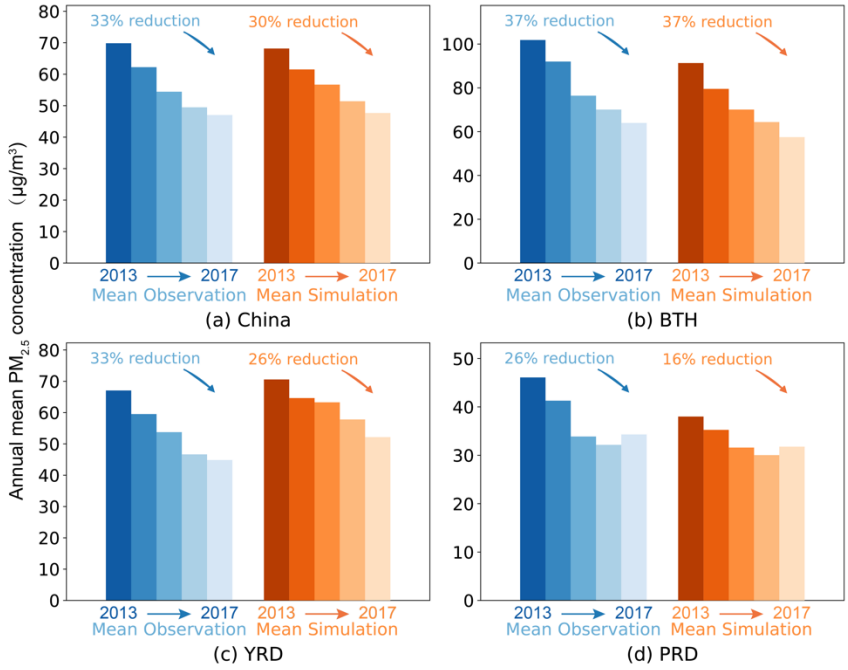

Fig. S3 Regional-averaged annual mean $PM_{2.5}$ observations and simulations from 2013 to 2017 for (a) China, (b) BTH, (c) YRD, and (d) PRD. Simulations were sampled by observations spatially and temporally.

Fig. S4.

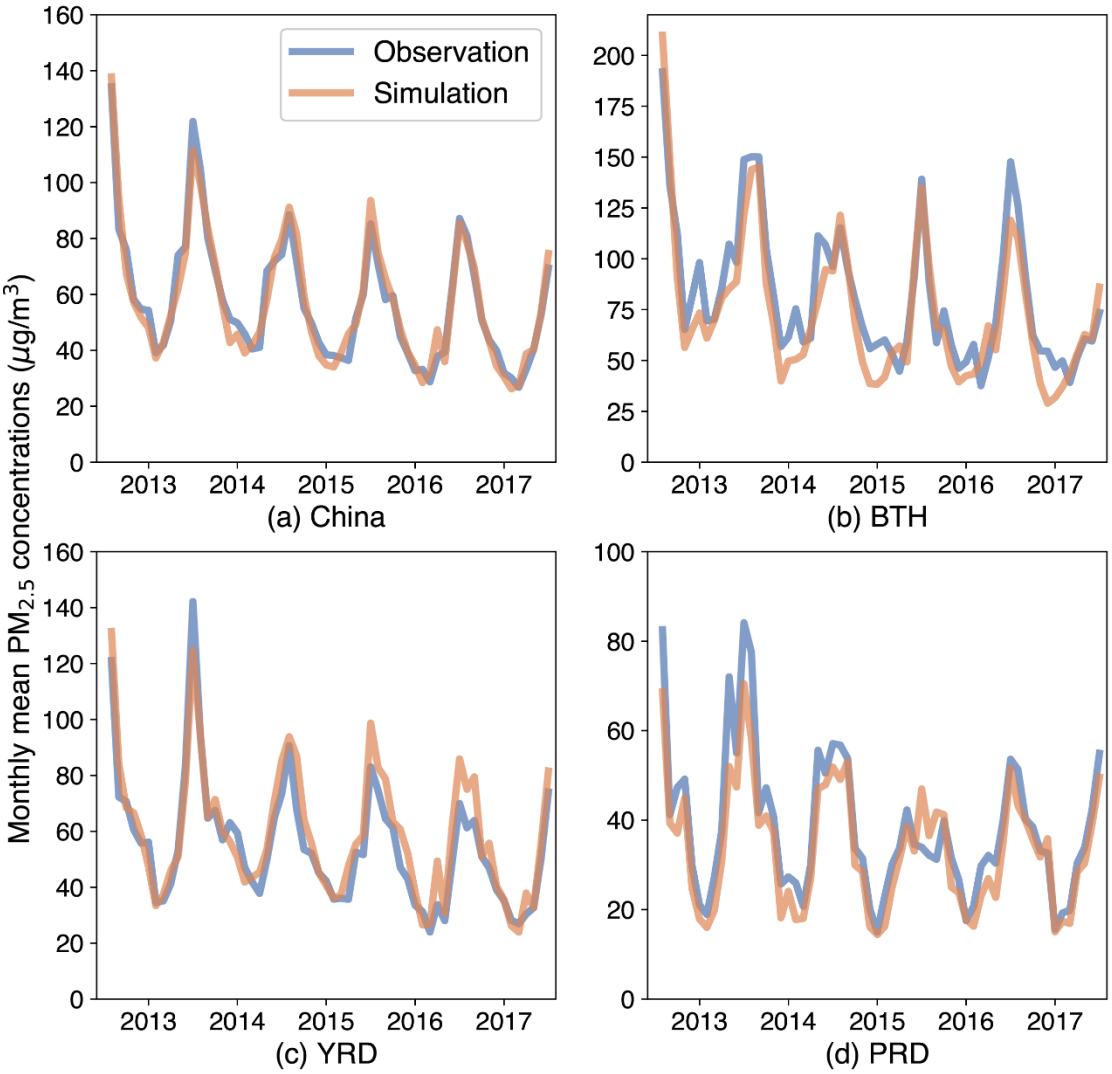

Fig. S4 Comparison between simulated and observed monthly mean $PM_{2.5}$ concentrations for (a) China, (b) BTH, (c) YRD, and (d) PRD from 2013 to 2017. Simulations were sampled with observations.

Fig. S5.

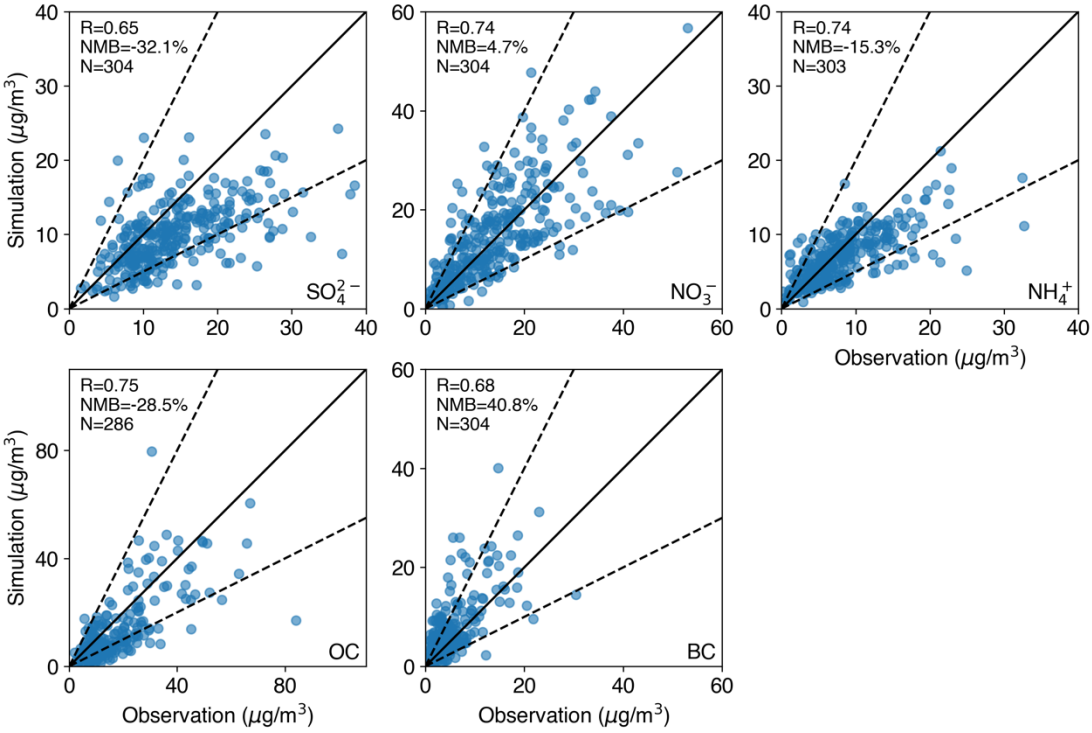

Fig. S5 Evaluation of simulated $PM_{2.5}$ chemical composition concentrations against ground-based observations. The solid line corresponds to the 1:1 line, and the dashed lines correspond to the 1:2 and 2:1 lines. R, NMB, and N stand for the correlation coefficient, normalized mean bias, and sample number, respectively.

Fig. S6.

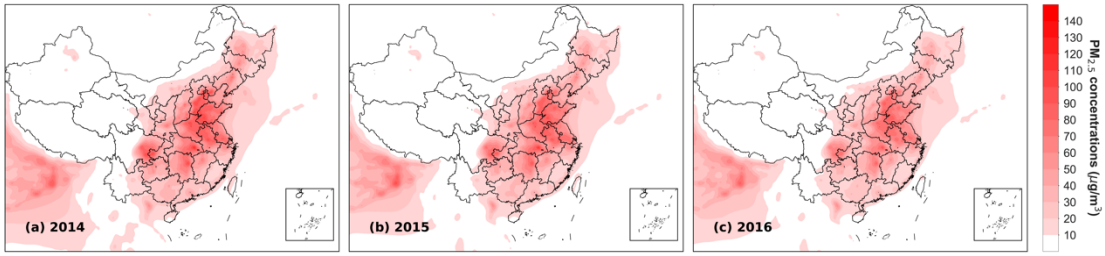

Fig. S6 Spatial distribution of annual mean $PM_{2.5}$ concentrations in China for (a) 2014, (b) 2015, and (c) 2016.

Fig. S7.

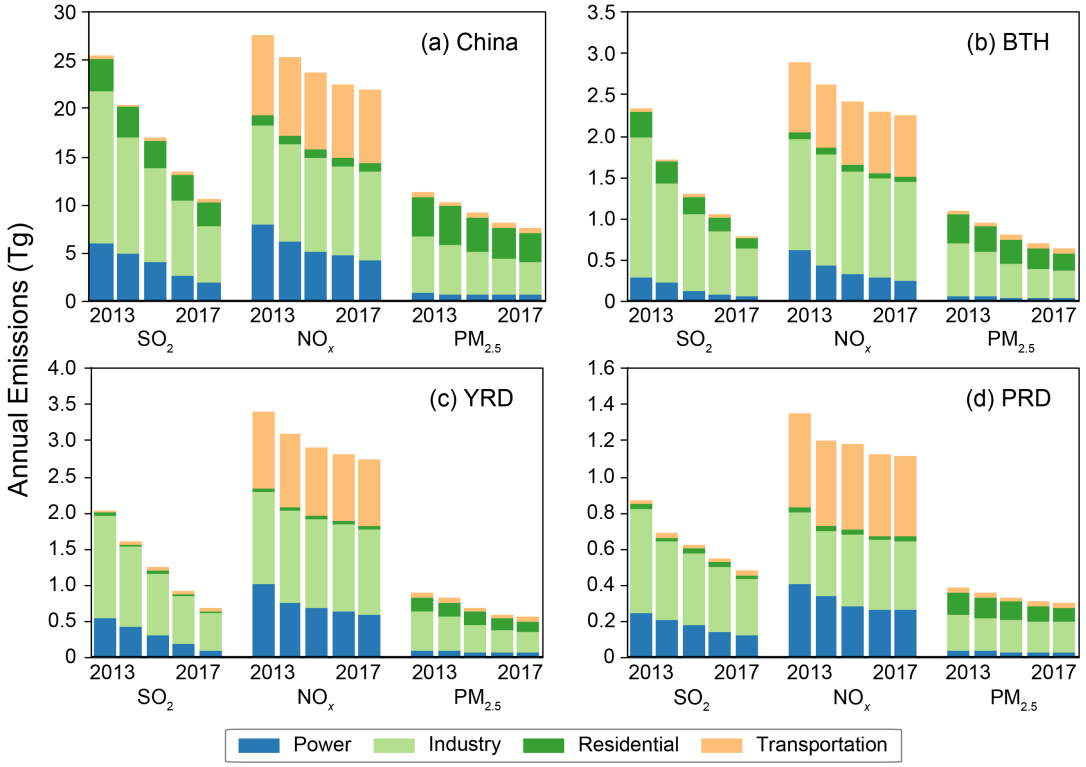

Fig. S7 Sectoral emission of SO_2, NO_x, and $PM_{2.5}$ from 2013 to 2017 in (a) China, (b) BTH, (c) YRD, and (d) PRD.

Fig. S8.

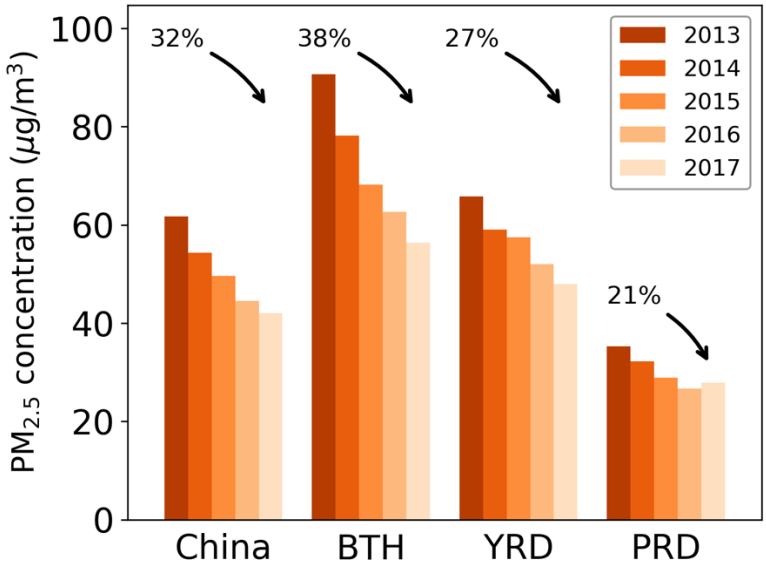

Fig. S8 Annual population-weighted mean $PM_{2.5}$ concentrations in China and the three key regions from 2013 to 2017. Labels over bars depict reduction ratios of simulated $PM_{2.5}$ concentration for each region from 2013 to 2017.

Fig. S9.

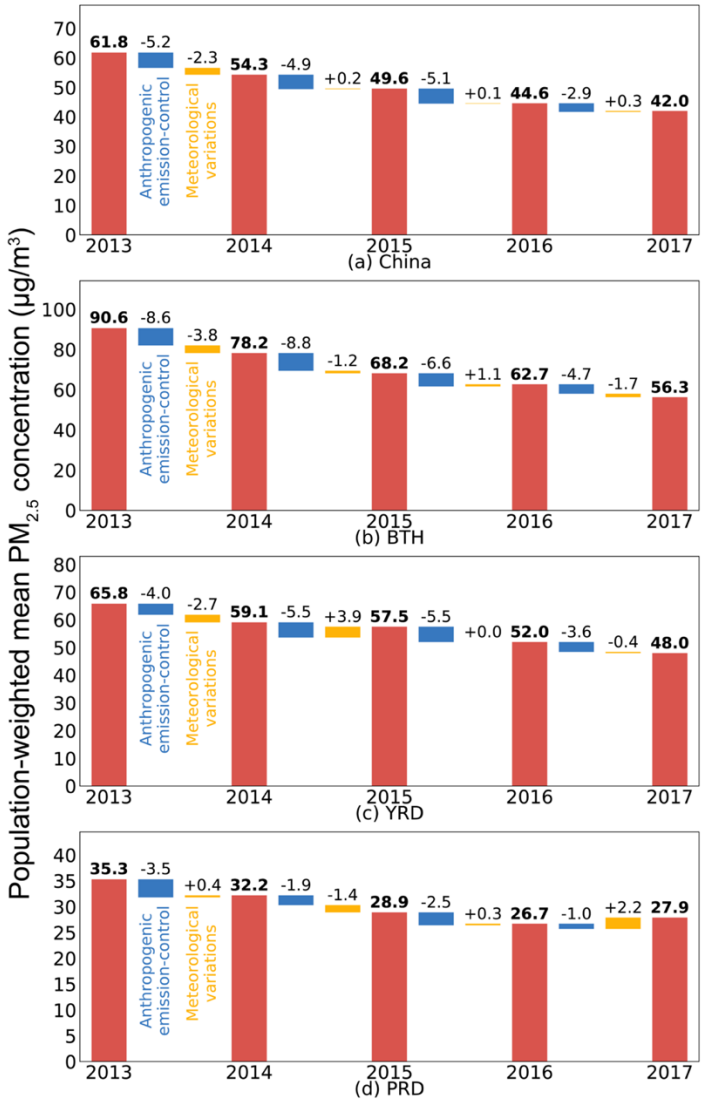

Fig. S9 Changes in annual population-weighted mean $PM_{2.5}$ concentrations contributed by anthropogenic emission control (blue bars) and meteorological condition changes (yellow bars) between 2013 and 2017 for (a) China, (b) BTH, (c) YRD, and (d) PRD.

Fig. S10.

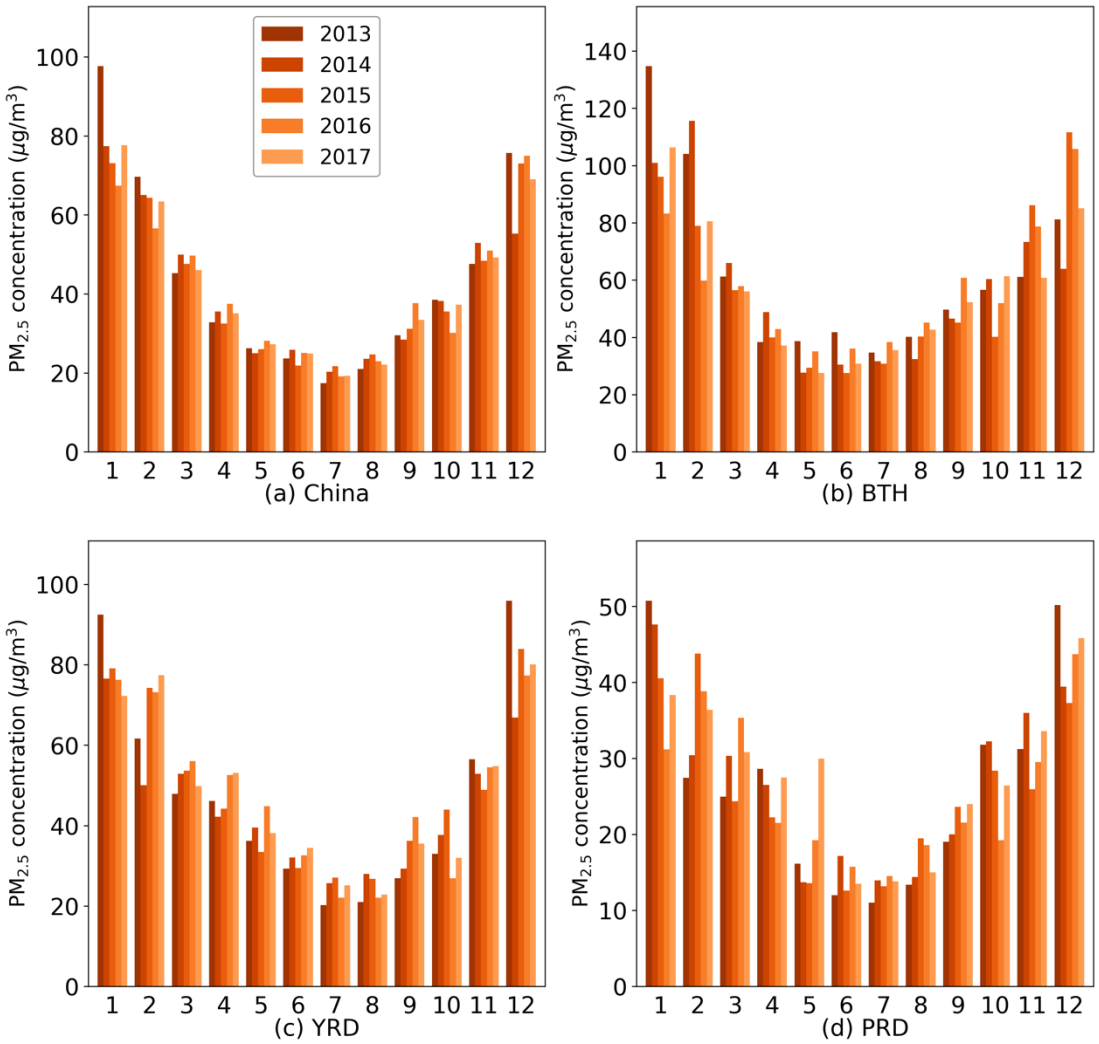

Fig. S10 Variations in monthly population-weighted mean $PM_{2.5}$ concentrations driven by varying meteorological conditions and fixed emissions in 2017 over 2013-2017 for (a) China, (b) BTH, (c) YRD, (d) PRD.

Fig. S11.

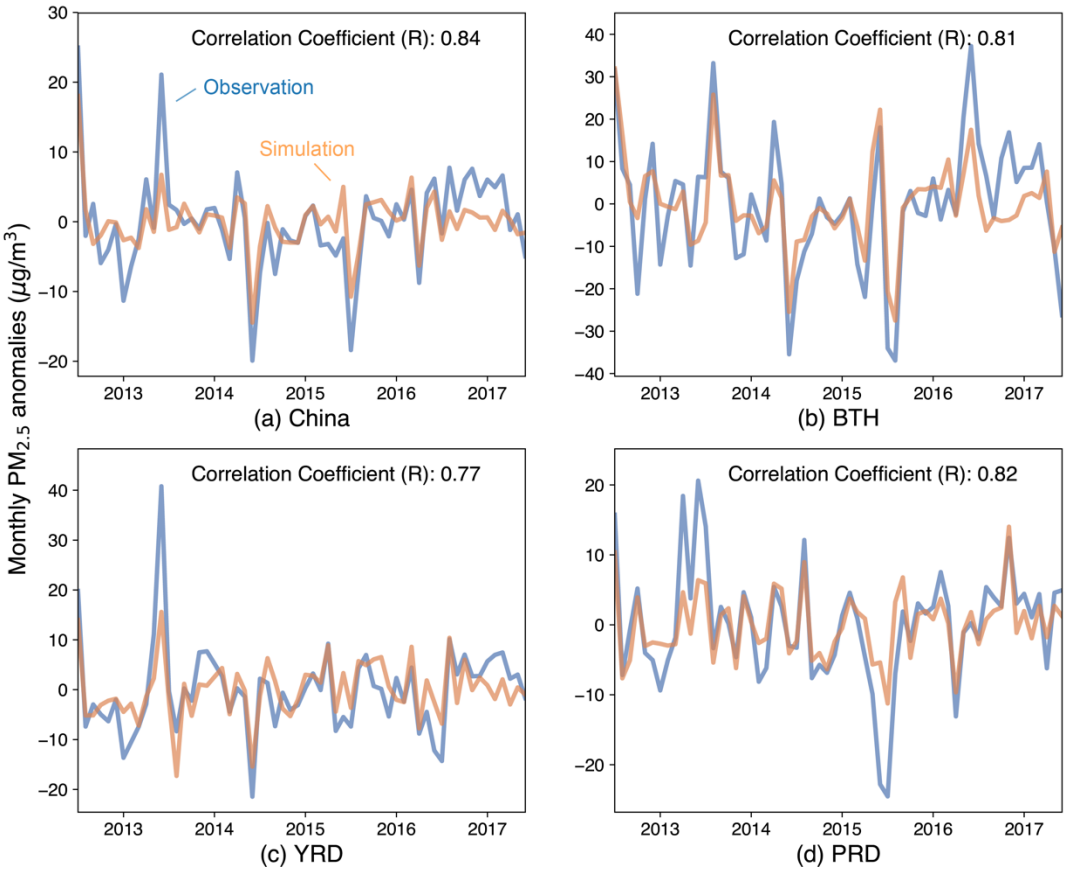

Fig. S11 Time series of monthly anomalies of detrended $PM_{2.5}$ observations and $PM_{2.5}$ concentrations simulated in the *FixEmis* scenario relative to their 2013–2017 means for individual months in China and the three key regions. (a) China, (b) BTH, (c) YRD, (d) PRD. Simulations were sampled with observations.

Fig. S12.

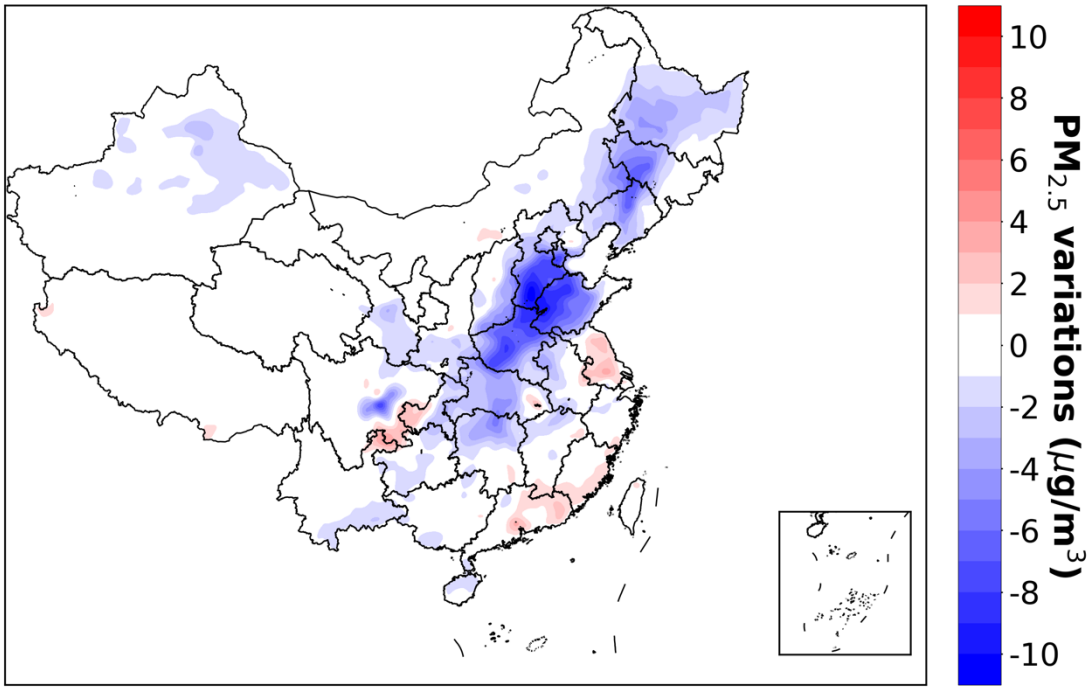

Fig. S12 Map of changes in annual mean $PM_{2.5}$ concentrations induced by interannual variations in meteorological conditions between 2013 and 2017.

Fig. S13.

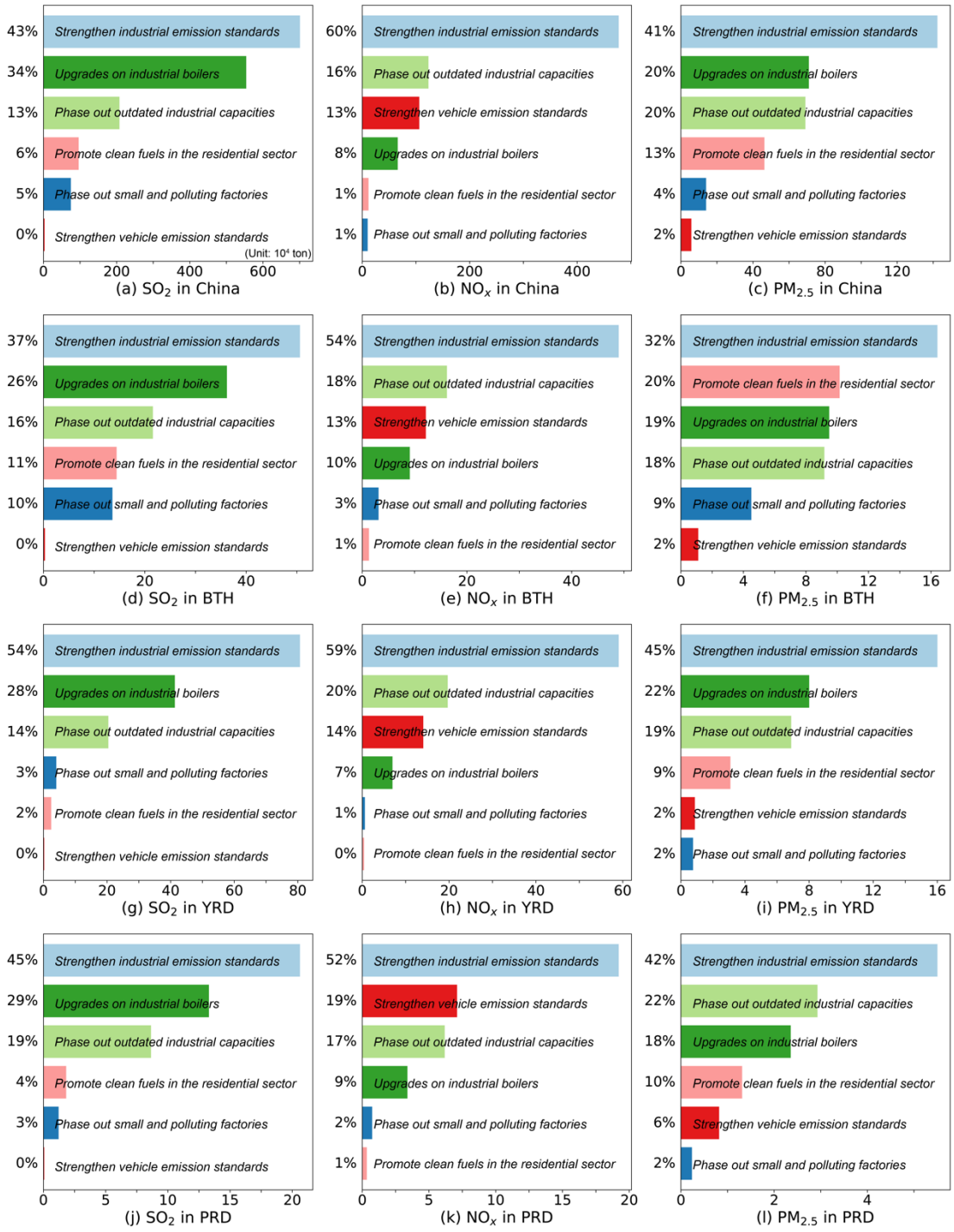

Fig. S13 Emission reductions in SO_2, NO_x, and $PM_{2.5}$ obtained in 2017 contributed by the five-year implementation of the six clean air measures (unit: 10^4 ton) over China and the three key regions. The tick labels on the y-axis depict the fraction of emission reductions contributed by each measure out of the total emission.

Fig. S14.

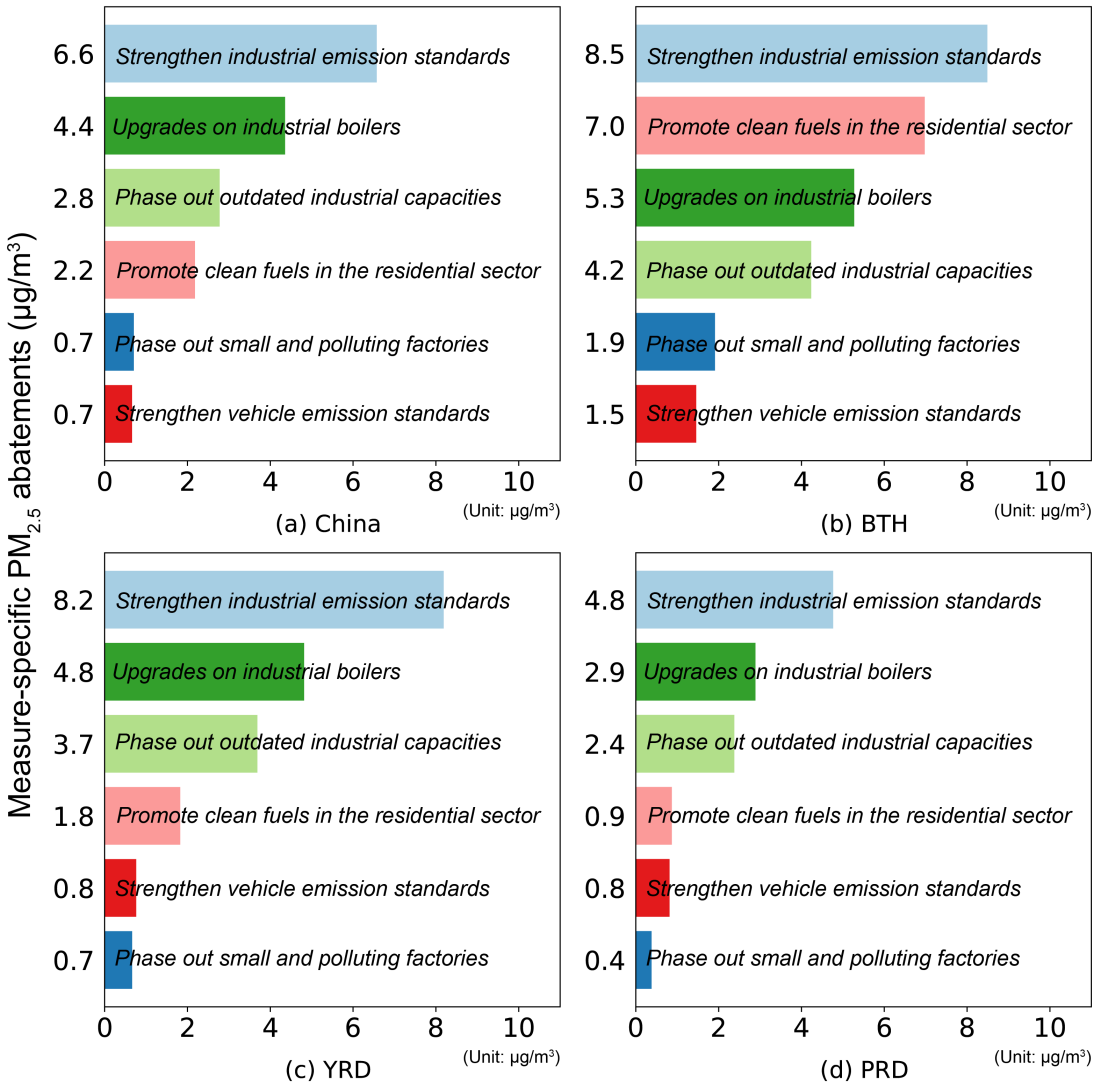

Fig. S14 Contribution of $PM_{2.5}$ abatements from the six control measures for (a) China, (b) BTH, (c) YRD, and (d) PRD.

Fig. S15.

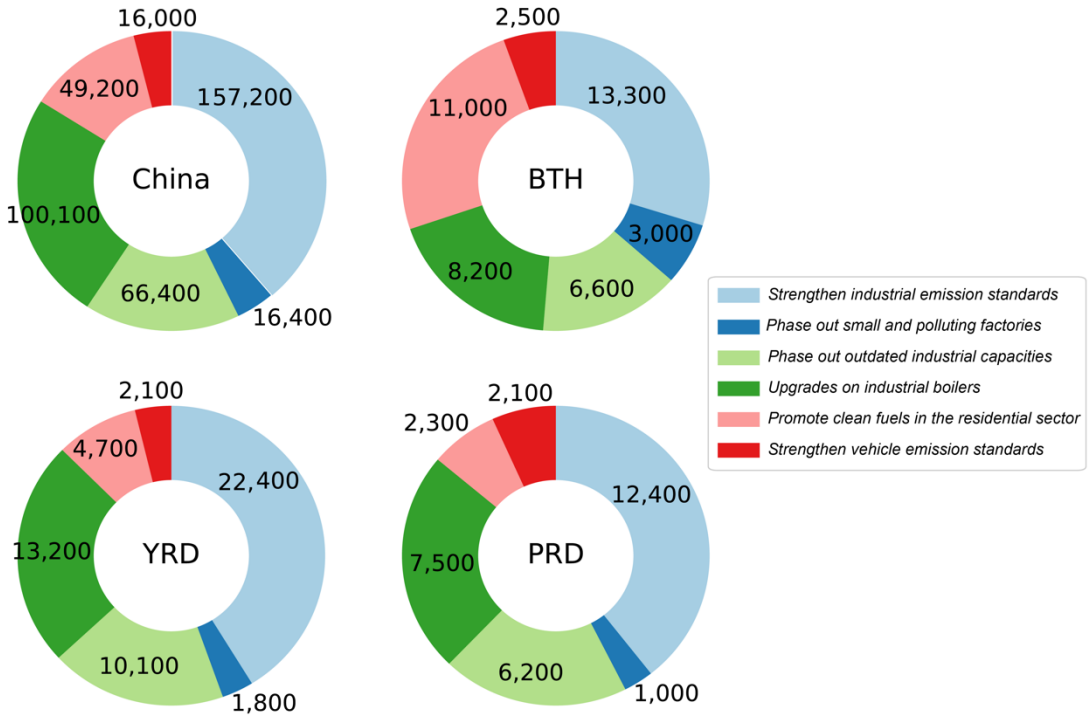

Fig. S15 Avoided $PM_{2.5}$-attributable premature mortalities from the six clean air measures at a national scale and over the three key regions. Labels depict the avoided excess deaths introduced by the individual measure.

Fig. S16.

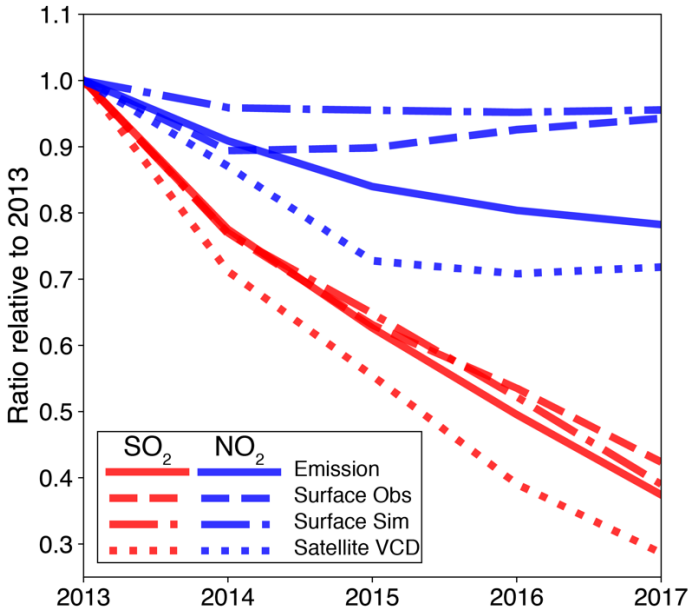

Fig. S16 Comparison of emission trends, model simulation trends, and observation trends from both ground and space for SO_2 (red lines) and NO_2 (blue lines) during 2013-2017 over Eastern China. Solid lines, dashed lines, dash-dot lines, and dotted lines represent emissions, ground observations, model simulations, and satellite vertical column densities from OMI, respectively. Eastern China here includes the provinces of Beijing, Tianjin, Hebei, Shanxi, Shaanxi, Shandong, Henan, Hubei, Anhui, Jiangsu, Shanghai, and Zhejiang.

Fig. S17.

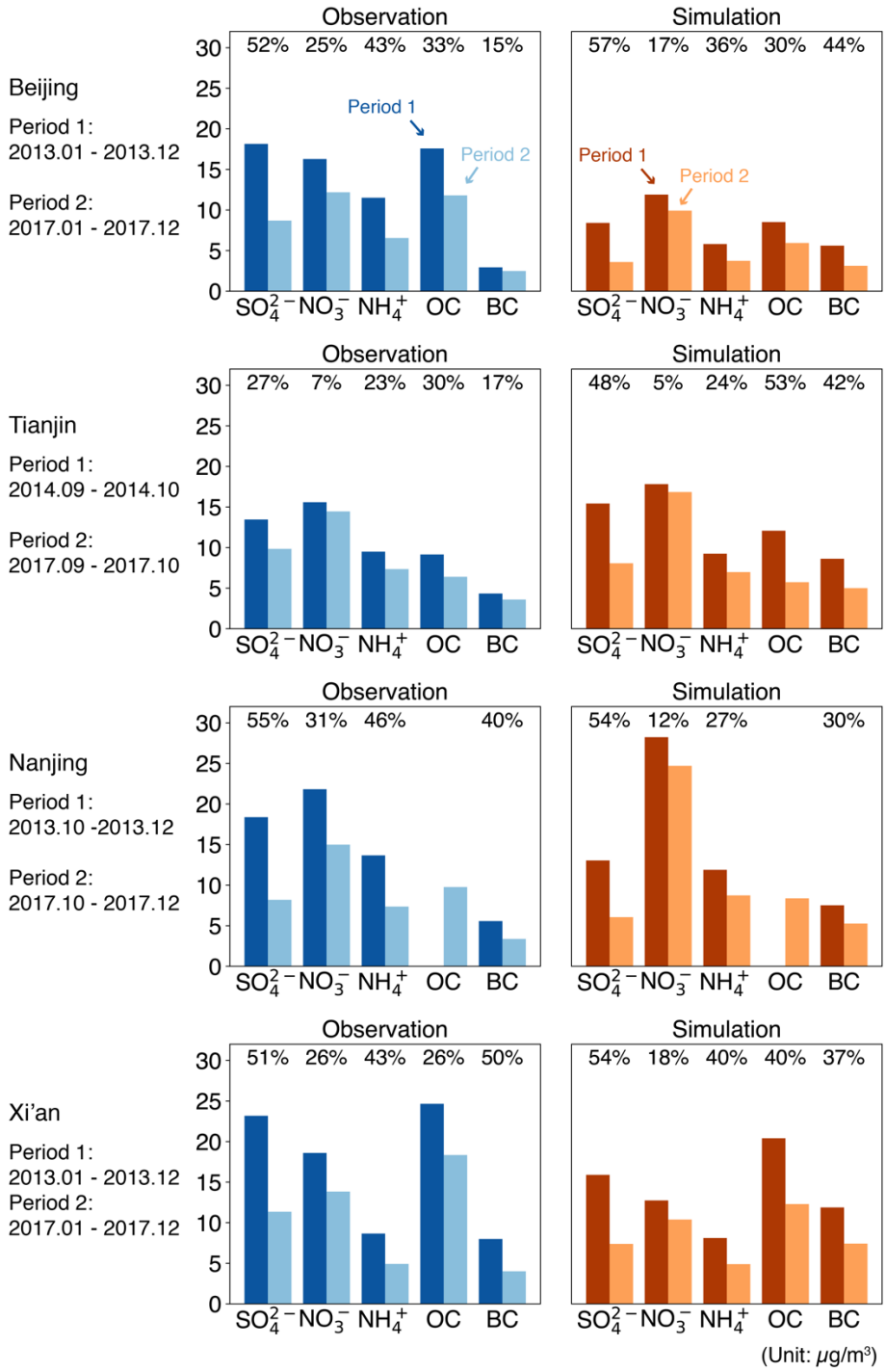

Fig. S17 Comparison of simulated and observed concentration changes in $PM_{2.5}$ chemical compositions in Beijing, Tianjin, Nanjing, and Xi'an. Information on observation sites is presented in Table S2. Values over bars show the percentage decreases in $PM_{2.5}$ chemical compositions during the two periods as defined for each city.

Fig. S18.

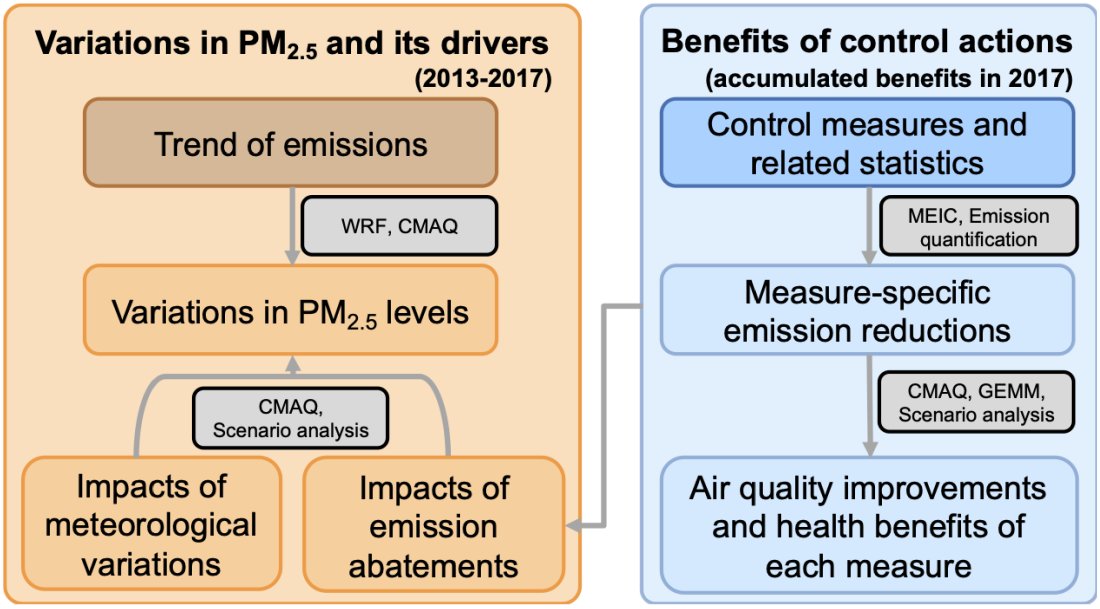

Fig. S18 Methodology framework for this study. This framework consists of two parts: an evaluation of $PM_{2.5}$ variation and anthropogenic and meteorological drivers of $PM_{2.5}$ variations from 2013 to 2017 (left panel) and estimation of the benefits of each emission control measure (right panel). The WRF model, CMAQ model, MEIC model, and GEMM functions represent the Weather Research and Forecasting Model, Community Multiscale Air Quality Model, the Multi-resolution Emission Inventory for China, and the Global Exposure Mortality Model, respectively.

Fig. S19.

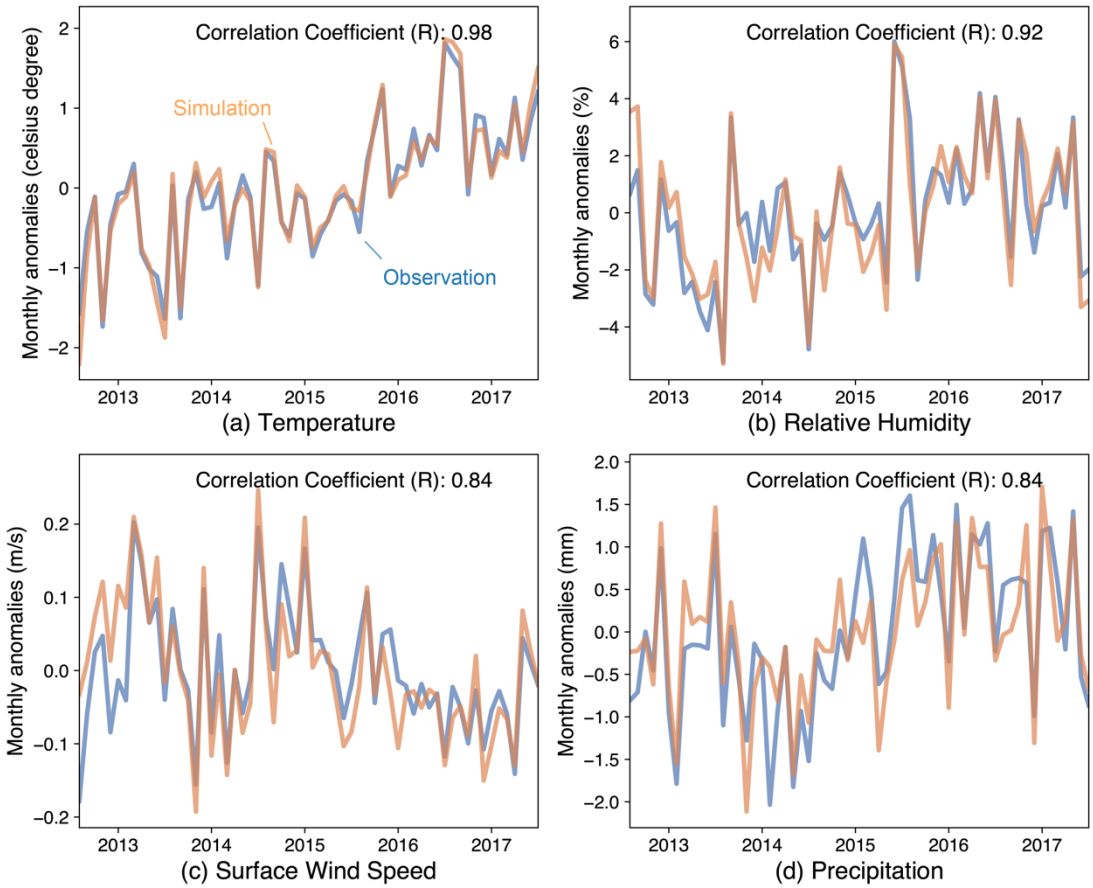

Fig. S19 Time series of monthly anomalies of four major meteorological parameters relative to their 2013–2017 means for individual months in China. (a) Temperature, (b) relative humidity, (c) surface wind speed, (d) daily precipitation. Simulations were sampled with observations.

Fig. S20.

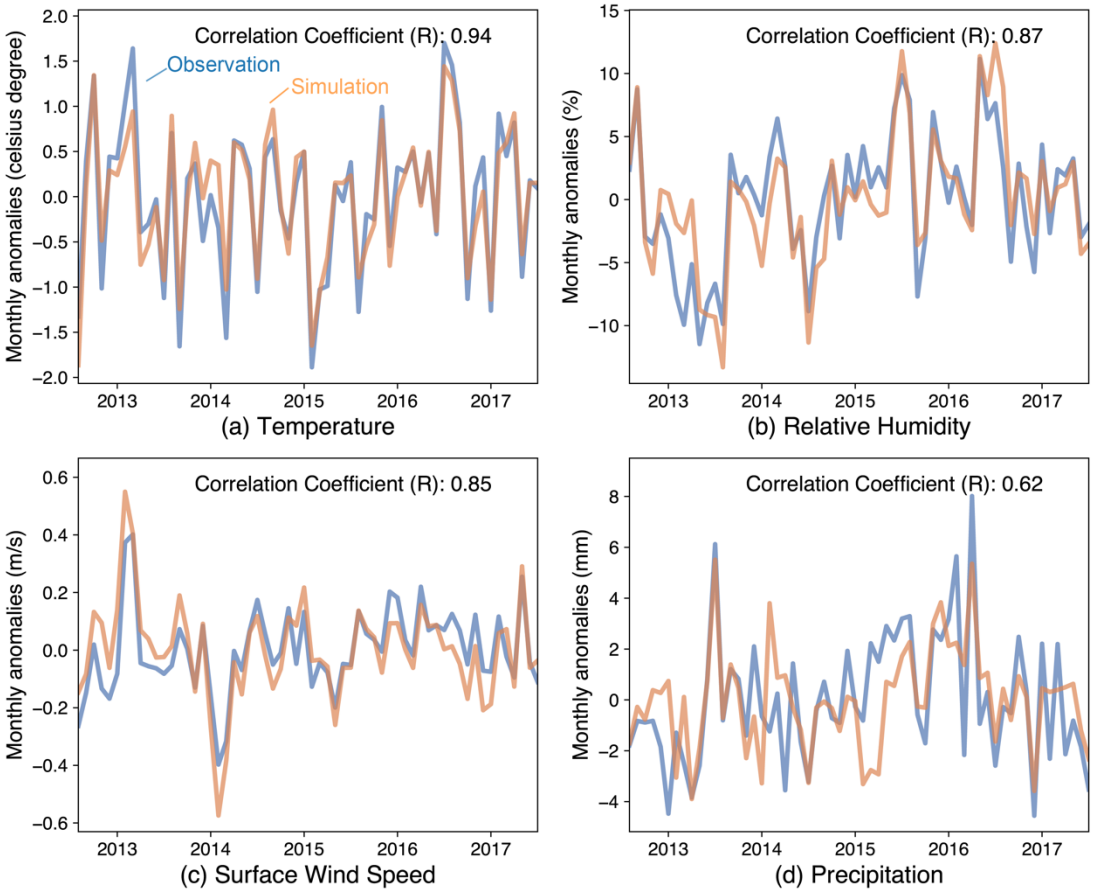

Fig. S20 Time series of monthly anomalies of four major meteorological parameters relative to their 2013–2017 means for individual months in the BTH region. (a) Temperature, (b) relative humidity, (c) surface wind speed, (d) daily precipitation. Simulations were sampled with observations.

Fig. S21.

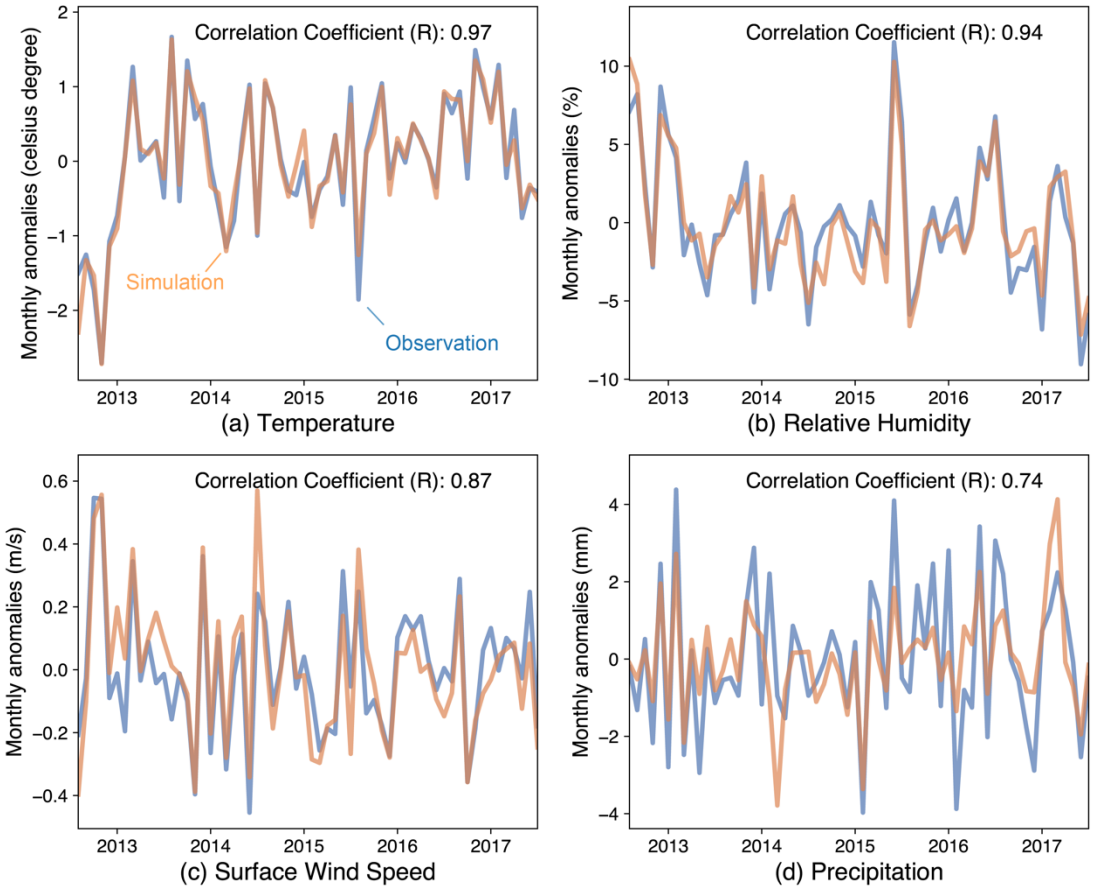

Fig. S21 Time series of monthly anomalies of four major meteorological parameters relative to their 2013–2017 means for individual months in the YRD region. (a) Temperature, (b) relative humidity, (c) surface wind speed, (d) daily precipitation. Simulations were sampled with observations.

Fig. S22.

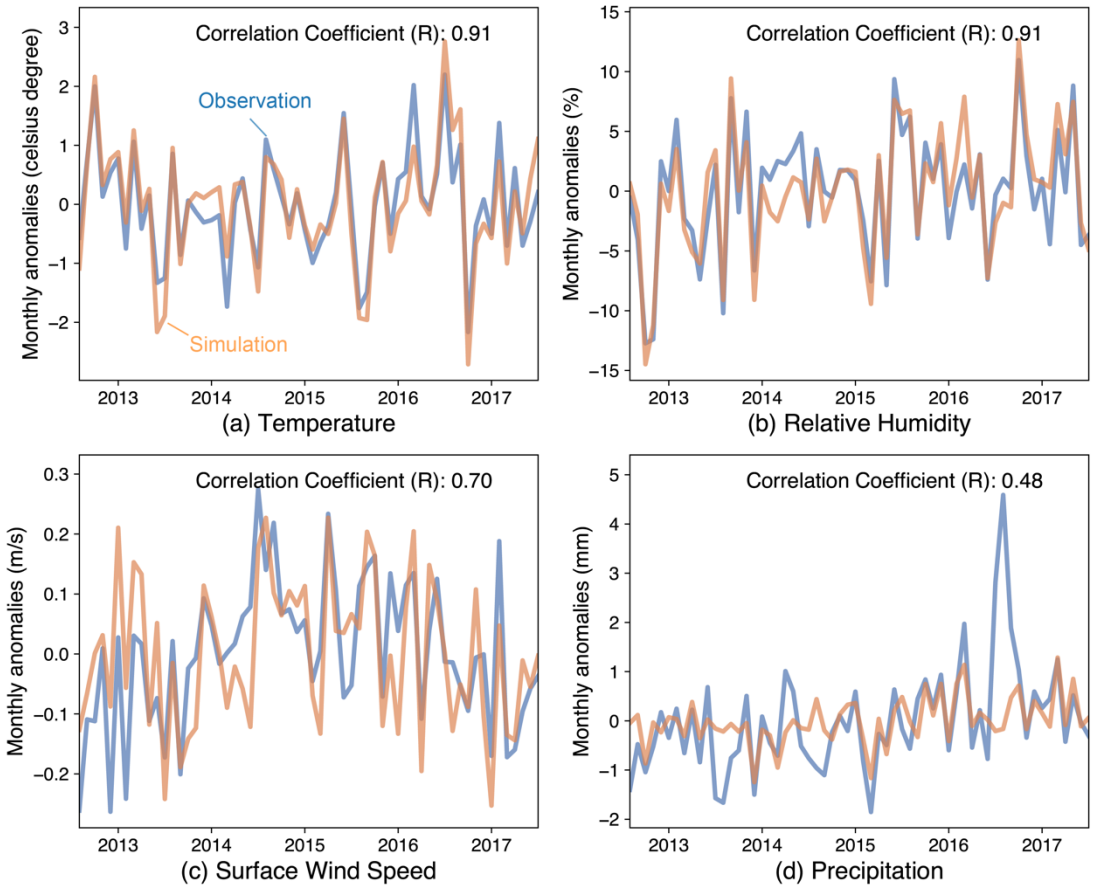

Fig. S22 Time series of monthly anomalies of four major meteorological parameters relative to their 2013–2017 means for individual months in the PRD region. (a) Temperature, (b) relative humidity, (c) surface wind speed, (d) daily precipitation. Simulations were sampled with observations.

List of Tables

Table S1. List of scenario groups.

Cases	Number of subcases	Year of meteorology	Anthropogenic emissions	Notes
BASE	5	2013-2017	Baseline anthropogenic emissions for 2013-2017	Baseline simulation
FixEmis	4	2013-2016	Baseline anthropogenic emissions for 2017	To quantify impacts of variations in meteorology
MEAS	6	2017	Baseline anthropogenic emissions for 2017 plus the emission reductions from each of the six major control measures	To quantify impacts of each measure
NoCtrl	1	2017	Baseline anthropogenic emissions for 2017 plus the total emission reductions from the six major control measures	For normalization

Table S2. Summary of $PM_{2.5}$ composition observations.

Region	City	Data Source	Time samples	Latitude	Longitude	Period of observation	Temporal resolution
BTH	Beijing	Collected in this study, measured by Beijing Municipal Environmental Monitoring Center (30, 31)	36	39.99	116.32	2013, 2015, 2017	Monthly mean
	Beijing	Ji et al., 2016 (32)	1	39.97	116.37	2013.03-2014.02	Annual mean
	Beijing	Yang et al., 2016 (33)	1	39.97	116.37	2013.11-12, 2014.11-12	Monthly mean
	Beijing	Tao et al., 2015 (34)	2	40.03	116.4	2013.01	Monthly mean
	Beijing	Lin et al., 2016 (35)	1	39.97	116.37	2014.02-2014.03	Monthly mean
	Beijing	Huang et al., 2014 (36)	1	39.99	116.39	2013.01	Monthly mean
	Tianjin	Collected in this study, measured by Institute of Atmospheric Physics, CAS (37)	13	39.08	117.21	2014-2017	Monthly mean
	Tianjin	Wang et al., 2016a (38)	1	39.17	117.17	2013.12-2014.01	Monthly mean
	Shijiazhuang	Collected in this study, measured by Institute of Atmospheric Physics, CAS (37)	4	38.03	114.47	2015.01-2016.01	Monthly mean
	Baoding	Collected in this study, measured by Chinese Research Academy of Environmental Sciences (39)	4	38.87	115.47	2014.01-2014.11	Monthly mean

	Langfang	Collected in this study, measured by Chinese Research Academy of Environmental Sciences (39)	4	39.54	116.71	2013.12-2014.10	Monthly mean
	Handan	Wei et al., 2014 (40)	1	36.58	114.51	2013.01	Monthly mean
	Gucheng	Collected in this study, measured by Chinese Academy of Meteorological Sciences (41)	1	39.13	115.8	2016	Annual mean
YRD	Shanghai	Collected in this study, measured by Shanghai Environmental Monitoring Center (42, 43)	12	31.23	121.53	2016.01-2016.12	Monthly mean
	Shanghai	Collected in this study, measured by Shanghai Environmental Monitoring Center (42, 43)	12	31.09	120.98	2016.01-2016.12	Monthly mean
	Shanghai	Ming et al., 2017 (44)	5	31.3	121.51	2013.09-2014.08	Seasonal and annual mean
	Shanghai	Chang et al., 2017 (45)	2	31.23	121.54	2013-2014	Annual mean
	Shanghai	Huang et al., 2014 (36)	1	31.3	121.5	2013.01	Monthly mean
	Nanjing	Collected in this study, measured by Nanjing University (46)	56	32.1	118.97	2013-2017	Monthly mean
	Hangzhou	Collected in this study, measured by Institute of Earth Environment, CAS (47)	2	30.29	120.17	2013.01, 2013.07	Monthly mean

	Lin'an	Collected in this study, measured by Chinese Academy of Meteorological Sciences (41)	1	30.3	119.73	2016	Annual mean
PRD	Guangzhou	Collected in this study, measured by Institute of Earth Environment, CAS (47)	2	23.15	113.51	2013.01, 2013.07	Monthly mean
	Guangzhou	Tao et al., 2017 (48)	4	23.12	113.35	2014.01-2014.12	Seasonal and annual mean
	Guangzhou	Cui et al., 2015 (49)	2	23.13	113.27	2013.06-07, 2013.11-12	Monthly mean
	Guangzhou	Huang et al., 2014 (36)	1	23.12	113.36	2013.01	Monthly mean
	Zhuhai	Tao et al., 2017 (48)	4	22.37	113.53	2014	Seasonal and annual mean
Other Regions	Shenyang	Collected in this study, measured by Chinese Research Academy of Environmental Sciences (39)	4	41.79	123.44	2015.01-2015.10	Monthly mean
	Dalian	Collected in this study, measured by Chinese Research Academy of Environmental Sciences (39)	4	38.95	121.62	2013.05-2014.03	Monthly mean
	Changchun	Collected in this study, measured by Institute of Earth Environment, CAS (47)	2	43.82	125.34	2013.01, 2013.07	Monthly mean

Harbin	Collected in this study, measured by Chinese Research Academy of Environmental Sciences (39)	4	45.74	126.64	2013.12-2014.10	Monthly mean
Longfengshan	Collected in this study, measured by Chinese Academy of Meteorological Sciences (41)	1	44.73	127.6	2016	Annual mean
Jinan	Collected in this study, measured by Nanjing University (46)	11	36.67	117.06	2013.01-2014.05	Monthly mean
Qingdao	Collected in this study, measured by Institute of Earth Environment, CAS (47)	2	36	120.3	2013.01, 2013.07	Monthly mean
Xiamen	Collected in this study, measured by Institute of Earth Environment, CAS (47)	4	24.51	118.15	2013.01-2013.10	Monthly mean
Nanning	Collected in this study, measured by Chinese Academy of Meteorological Sciences (41)	1	22.8	108.32	2016	Annual mean
Sanya	Wang et al., 2015 (50)	1	18.3	109.52	2013.06-2013.07	Monthly mean
Haikou	Liu et al., 2017 (51)	4	20	110.34	2015.01-2015.09	Monthly mean
Zhengzhou	Collected in this study, measured by Chinese Research Academy of Environmental Sciences (39)	4	34.79	113.65	2015.01-2015.10	Monthly mean
Zhengzhou	Wang et al., 2016b (52)	1	34.82	113.54	2013.01-2013.12	Annual mean
Zhengzhou	Wang et al., 2017 (53)	1	34.82	113.54	2014.10-2015.07	Monthly mean

Xinxiang	Feng et al., 2016 (54)	1	35.32	113.91	2015.02	Monthly mean
Taiyuan	Collected in this study, measured by Institute of Earth Environment, CAS (47)	2	37.85	112.52	2013.01, 2013.07	Monthly mean
Hefei	Collected in this study, measured by Chinese Research Academy of Environmental Sciences (39)	4	31.85	117.24	2014.04-2014.12	Monthly mean
Suixi	Li et al., 2014 (55)	1	33.91	116.76	2013.06-2013.07	Monthly mean
Wuhan	Collected in this study, measured by Institute of Earth Environment, CAS (47)	1	30.52	114.4	2013.07	Monthly mean
Jinsha	Collected in this study, measured by Chinese Academy of Meteorological Sciences (41)	1	29.63	114.2	2016	Annual mean
Changde	Collected in this study, measured by Chinese Academy of Meteorological Sciences (41)	1	29.17	111.71	2016	Annual mean
Chongqing	Collected in this study, measured by Sichuan University (56)	5	29.62	106.51	2015.01-2016.01	Monthly mean
Chongqing	Zhang et al., 2015b (57)	4	30.8	108.4	2013.01-2013.10	Monthly mean
Chengdu	Collected in this study, measured by Institute of Earth Environment, CAS (47)	2	30.66	104.02	2013.01, 2013.07	Monthly mean

Kunming	Collected in this study, measured by Chinese Research Academy of Environmental Sciences (39)	1	25.012	102.7	2014.01	Monthly mean
Xi'an	Collected in this study, measured by Institute of Earth Environment, CAS (47)	60	34.23	108.89	2013.01-2017.12	Monthly mean
Xi'an	Huang et al., 2014 (36)	1	34.23	108.88	2013.01	Monthly mean
Yulin	Collected in this study, measured by Institute of Earth Environment, CAS (47)	2	38.3	109.9	2013.01, 2013.07	Monthly mean
Yinchuan	Collected in this study, measured by Chinese Research Academy of Environmental Sciences (39)	4	38.5	106.14	2013.12-2014.10	Monthly mean
Lanzhou	Tan et al., 2016 (58)	1	36.05	103.83	2013.06-2013.07	Monthly mean
Jinchang	Collected in this study, measured by Institute of Earth Environment, CAS (47)	1	38.3	101.1	2013.07	Monthly mean
Gaolanshan	Collected in this study, measured by Chinese Academy of Meteorological Sciences (41)	1	36	105.85	2016	Annual mean
Xining	Collected in this study, measured by Chinese Research Academy of Environmental Sciences (39)	3	36.65	101.71	2014.02-2014.09	Monthly mean

Urumqi	Collected in this study, measured by Institute of Earth Environment, CAS (47)	1	43.87	87.56	2013.07	Monthly mean

Note: $PM_{2.5}$ composition data listed in this table are available in SI dataset. For data collected in this study, details on the sampling approach and chemical analyzes are documented in the corresponding references.

Table S3. Evaluation of $PM_{2.5}$ concentrations simulated by the CMAQ model.

Region	Year	Sample Number	R	Mean Observation	Mean Simulation	MB	RMSE	NMB	NME
China	2013	25087	0.73	69.8	67.4	-2.4	42.3	-3.5	38.3
	2014	26347	0.72	62.2	60.9	-1.4	35.6	-2.2	37.9
	2015	26935	0.73	54.4	56.1	1.6	33.3	3.0	40.3
	2016	27084	0.69	49.5	50.9	1.4	33.2	2.8	42.6
	2017	26934	0.70	47.0	47.2	0.1	30.1	0.3	41.0
BTH	2013	4388	0.70	101.9	91.7	-10.2	58.9	-10.0	35.3
	2014	4631	0.77	92.0	79.8	-12.2	48.8	-13.2	33.8
	2015	4732	0.75	76.4	70.3	-6.1	43.1	-8.0	37.1
	2016	4758	0.74	70.1	64.6	-5.5	41.7	-7.8	36.8
	2017	4732	0.75	64.0	57.7	-6.2	35.3	-9.8	36.1
YRD	2013	7761	0.79	67.1	66.7	-0.4	33.0	-0.5	33.3
	2014	8188	0.74	59.5	61.1	1.5	27.6	2.6	33.5
	2015	8371	0.80	53.7	59.8	6.1	26.3	11.3	35.3
	2016	8418	0.79	46.6	54.6	8.0	28.0	17.1	40.6
	2017	8372	0.80	44.8	49.3	4.5	22.8	9.9	36.3
PRD	2013	3177	0.77	46.1	38.1	-7.9	20.7	-17.2	32.8
	2014	3204	0.75	41.3	35.4	-5.9	18.1	-14.3	32.0
	2015	3276	0.76	33.9	31.7	-2.2	15.2	-6.4	33.0
	2016	3294	0.71	32.2	30.1	-2.0	14.9	-6.2	35.2
	2017	3274	0.69	34.3	31.9	-2.4	16.1	-7.0	33.7
Other Regions	2013	9761	0.68	65.4	66.6	1.2	45.0	1.9	45.8
	2014	10324	0.65	57.5	60.1	2.5	38.3	4.4	45.7
	2015	10556	0.65	51.5	54.3	2.8	37.1	5.4	48.0
	2016	10614	0.59	47.9	48.1	0.2	36.7	0.5	49.5
	2017	10556	0.61	45.1	45.5	0.3	35.4	0.7	49.5

Note: Units for Mean Observation, Mean Simulation, MB (Mean Bias), RMSE (Root Mean Squared Error), NMB (Normalized Mean Bias), and NME (Normalized Mean Error) are $\mu g/m^3$, $\mu g/m^3$, $\mu g/m^3$, $\mu g/m^3$, %, and %, respectively.

Table S4. Emission reductions in 2017 compared to 2013 from each of the six major measures in China's clean air action (Tg).

	China			BTH		
Measures	SO_2	NO_x	$PM_{2.5}$	SO_2	NO_x	$PM_{2.5}$
Strengthen industrial emission standards	7.01	4.77	1.42	0.51	0.49	0.16
Phase out small and polluting factories	0.75	0.1	0.14	0.14	0.03	0.05
Phase out outdated industrial capacities	2.08	1.23	0.69	0.22	0.16	0.09
Upgrades on industrial boilers	5.54	0.66	0.71	0.36	0.09	0.09
Promote clean fuels in the residential sector	0.96	0.12	0.46	0.14	0.01	0.1
Strengthen vehicle emission standards	0.03	1.06	0.06	0	0.12	0.01
Total	16.37	7.95	3.48	1.37	0.91	0.51
	YRD			PRD		
Measures	SO_2	NO_x	$PM_{2.5}$	SO_2	NO_x	$PM_{2.5}$
Strengthen industrial emission standards	0.81	0.59	0.16	0.21	0.19	0.06
Phase out small and polluting factories	0.04	0.01	0.01	0.01	0.01	0
Phase out outdated industrial capacities	0.2	0.2	0.07	0.09	0.06	0.03
Upgrades on industrial boilers	0.41	0.07	0.08	0.13	0.03	0.02
Promote clean fuels in the residential sector	0.02	0	0.03	0.02	0	0.01
Strengthen vehicle emission standards	0	0.14	0.01	0	0.07	0.01
Total	1.49	1.01	0.36	0.46	0.37	0.13

Table S5. $PM_{2.5}$-attributable excess deaths in *BASE-2017* and *NoCtrl* scenarios estimated by three C-R models.

		BASE-2017 (95% CI)	*NoCtrl* (95% CI)	Reduction (95% CI)
GEMM (GEMM NCD+LRI)	China	1,975,400 (1,842,000, 2,094,800)	2,380,700 (2,233,600, 2,527,300)	405,300 (383,800, 425,000)
	BTH	199,500 (187,100, 212,100)	244,100 (228,500, 257,500)	44,600 (42,400, 46,500)
	YRD	264,200 (246,700, 281,100)	318,500 (299,400, 337,600)	54,300 (51,600, 56,800)
	PRD	128,500 (120,400, 136,600)	160,000 (149,100, 169,500)	31,500 (29,600, 33,100)
GEMM 5-COD	China	1,503,000 (1,635,300, 1,966,700)	1,805,900 (1,343,200, 1,641,800)	302,900 (276,400, 325,400)
	BTH	153,100 (165,500, 199,400)	184,200 (138,000, 167,300)	31,100 (28,500, 33,000)
	YRD	203,000 (219,100, 263,700)	242,600 (181,900, 221,500)	39,600 (36,100, 42,300)
	PRD	96,900 (110,300, 134,600)	122,600 (86,500, 106,400)	25,700 (23,300, 27,900)
IER	China	897,200 (769,500, 1,036,800)	1,027,800 (884,700, 1,172,700)	130,600 (115,900, 159,200)
	BTH	86,300 (74,600, 98,400)	100,000 (87,300, 113,000)	13,700 (12,100, 16,900)
	YRD	117,800 (99,800, 135,500)	134,200 (116,400, 151,500)	16,400 (14,400, 20,600)
	PRD	63,400 (53,300, 74,200)	73,900 (62,700, 85,900)	10,500 (9,100, 12,900)

Table S6. Summary of estimated parameters under the 2017 emission inventory and the uncontrolled scenario for each control measure.

No.	Measures	Sectors	Subsectors	Parameters in eq. 1	Targeted species	Production or control technologies	2017 emission inventory	2017 uncontrolled scenario
1	Strengthen industrial emission standards	Power sector	Coal-fired power plants	C'	SO_2	FGD (removal efficiency: 95%)	99.6%	84.5%
				C'	NO_x	LNB+SCR (or SNCR) (removal efficiency: 80%)	97.1%	42.6%
				C'	PM	ESP	54.0%	91.6%
				C'	PM	FAB	22.0%	6.4%
				C'	PM	ESP (or FAB)+WESP	24.0%	0.0%
		Iron and steel production	Sintering	C'	SO_2	FGD (removal efficiency: 85%)	80.4%	28.5%
				C'	PM	CYC	0.0%	1.2%
				C'	PM	WET	0.0%	12.1%
				C'	PM	ESP	20.0%	56.5%
				C'	PM	FAB	80.0%	30.1%
			Steel production (basic oxygen furnace)	C'	PM	CYC	0.0%	0.0%
				C'	PM	WET	0.0%	0.0%
				C'	PM	ESP	20.0%	2.0%
				C'	PM	FAB	80.0%	98.0%
			Steel production (electric arc furnace)	C'	PM	CYC	0.0%	4.9%
				C'	PM	WET	15.0%	46.2%
				C'	PM	ESP	35.0%	20.3%

				C'	PM	FAB	50.0%	28.6%
		Cement production	Precalciner kiln	C'	NO_x	LNB+SCR (or SNCR) (removal efficiency: 80%)	87.2%	35.2%
				C'	PM	ESP	7.0%	16.3%
				C'	PM	FAB	93.0%	83.0%
		Flat glass production	Float process	C'	SO_2	FGD (removal efficiency: 70%)	33.2%	0.0%
				C'	NO_x	LNB+SCR (or SNCR) (removal efficiency: 60%)	18.5%	0.0%
				C'	PM	CYC	0.0%	1.8%
				C'	PM	WET	0.0%	19.5%
				C'	PM	ESP	85.0%	73.5%
				C'	PM	FAB	15.0%	5.3%
2	Phase out small and polluting factories	Non-key industrial process	Foundry products	X'	All	Outdated technologies	20.0%	34.6%
			Non-ferrous metal	X'	All	Outdated technologies	6.0%	12.0%
			Lime production	X'	All	Traditional shaft kiln	30.0%	50.0%
			Brick production	X'	All	Traditional annular kiln	30.0%	50.0%
			Coke production	X'	All	Other coking oven	0.1%	6.7%

			Other industrial production	X'	All	Outdated production processes	4.2%	14.0%
			Foundry products	C'	PM	CYC	0.0%	30.0%
				C'	PM	WET	45.0%	30.0%
			Non-ferrous metal	C'	PM	CYC	0.0%	5.0%
				C'	PM	WET	0.5%	5.0%
			Lime production	C'	PM	CYC	5.0%	54.9%
				C'	PM	WET	40.0%	32.6%
			Brick production	C'	PM	NONE	0.0%	60.0%
				C'	PM	CYC	40.0%	35.0%
				C'	PM	WET	60.0%	5.0%
			Coke production	C'	PM	CYC	0.7%	1.5%
				C'	PM	WET	12.1%	55.1%
3	Phase out outdated industrial capacity	Power sector	Coal-fired power plants	A'	All	/	A-2017	1.02*A-2017
		Iron and steel production	Sintering production	A'	All	/	A-2017	1.13*A-2017
			Iron production	A'	All	/	A-2017	1.13*A-2017
			Steel production	A'	All	/	A-2017	1.13*A-2017
		Cement production	Cement production	A'	All	/	A-2017	1.11*A-2017
		Glass production	Flat glass production	A'	All	/	A-2017	1.09*A-2017
4		Industrial boilers		A'	All	/	A-2017	1.39*A-2017

	Upgrades on industrial boilers		Coal-fired industrial boilers	C'	SO_2	FGD (removal efficiency: 85%)	50.3%	0.5%
				C'	PM	CYC	1.2%	37.8%
				C'	PM	WET	80.0%	62.2%
				C'	PM	ESP	18.8%	0.0%
				C'	PM	FAB	0.0%	0.0%
5	Promote clean fuels in the residential sector	Residential sector	Coal	A'	All	/	A-2017	1.17*A-2017
			Natural gas	A'	All	/	A-2017	0.84*A-2017
			Raw coal	A'	All	/	30%*A-coal	44%*A'-coal
			Washed coal	A'	All	/	70%*A-coal	56%*A'-coal
			Residential urban	X'	All	Traditional stove	56.1%	66.0%
				X'	All	Advanced stove	43.9%	34.0%
			Residential rural	X'	All	Traditional stove	66.0%	100.0%
				X'	All	Advanced stove	34.0%	0.0%
6	Strengthen vehicle emission standards	On-road transportation	Heavy duty bus-diesel	X'	All	Pre-Euro1	0.0%	0.0%
				X'	All	Euro 1	0.0%	1.6%
				X'	All	Euro 2	1.1%	12.4%
				X'	All	Euro 3	29.8%	80.2%
				X'	All	Euro 4	46.0%	5.0%
				X'	All	Euro 5	23.0%	0.8%
			Medium duty bus-diesel	X'	All	Pre-Euro1	0.0%	0.0%
				X'	All	Euro 1	0.0%	5.3%

				X'	All	Euro 2	2.3%	24.7%
				X'	All	Euro 3	32.9%	61.4%
				X'	All	Euro 4	42.0%	7.1%
				X'	All	Euro 5	22.8%	1.4%
			Heavy duty truck-diesel	X'	All	Pre-Euro1	0.0%	0.0%
				X'	All	Euro 1	0.0%	0.6%
				X'	All	Euro 2	0.5%	8.5%
				X'	All	Euro 3	49.8%	88.8%
				X'	All	Euro 4	35.9%	1.8%
				X'	All	Euro 5	13.9%	0.3%
			Medium duty truck-diesel	X'	All	Pre-Euro1	0.0%	0.0%
				X'	All	Euro 1	0.0%	2.9%
				X'	All	Euro 2	2.2%	25.2%
				X'	All	Euro 3	59.9%	69.1%
				X'	All	Euro 4	27.2%	2.6%
				X'	All	Euro 5	10.8%	0.2%
			Light duty truck-diesel	X'	All	Pre-Euro1	0.0%	0.0%
				X'	All	Euro 1	0.0%	1.6%
				X'	All	Euro 2	1.4%	8.1%
				X'	All	Euro 3	35.0%	88.7%
				X'	All	Euro 4	62.1%	1.2%
				X'	All	Euro 5	1.4%	0.3%
			Mini truck-diesel	X'	All	Pre-Euro1	0.0%	0.0%
				X'	All	Euro 1	0.0%	20.8%

				X'	All	Euro 2	14.0%	35.2%
				X'	All	Euro 3	57.1%	44.0%
				X'	All	Euro 4	28.9%	0.0%
				X'	All	Euro 5	0.0%	0.0%
			Heavy duty bus-gasoline	X'	All	Pre-Euro1	0.0%	0.0%
				X'	All	Euro 1	0.0%	1.6%
				X'	All	Euro 2	5.4%	27.1%
				X'	All	Euro 3	16.8%	48.2%
				X'	All	Euro 4	72.5%	22.3%
				X'	All	Euro 5	5.2%	0.8%
			Medium duty bus-gasoline	X'	All	Pre-Euro1	0.0%	0.0%
				X'	All	Euro 1	0.0%	5.3%
				X'	All	Euro 2	8.8%	40.2%
				X'	All	Euro 3	17.7%	34.7%
				X'	All	Euro 4	64.6%	18.3%
				X'	All	Euro 5	8.9%	1.4%
			Light duty bus-gasoline	X'	All	Pre-Euro1	0.0%	0.5%
				X'	All	Euro 1	2.1%	5.4%
				X'	All	Euro 2	4.7%	7.4%
				X'	All	Euro 3	8.6%	29.4%
				X'	All	Euro 4	66.2%	56.4%
				X'	All	Euro 5	18.3%	1.0%
			Mini bus-gasoline	X'	All	Pre-Euro1	0.0%	0.0%
				X'	All	Euro 1	0.0%	34.8%

				X'	All	Euro 2	9.1%	11.1%
				X'	All	Euro 3	27.4%	29.0%
				X'	All	Euro 4	54.5%	24.9%
				X'	All	Euro 5	9.0%	0.2%
			Light duty truck-gasoline	X'	All	Pre-Euro1	0.0%	0.0%
				X'	All	Euro 1	0.0%	4.9%
				X'	All	Euro 2	1.4%	4.8%
				X'	All	Euro 3	9.3%	28.7%
				X'	All	Euro 4	71.4%	61.3%
				X'	All	Euro 5	17.8%	0.3%
			Mini truck-gasoline	X'	All	Pre-Euro1	0.0%	0.0%
				X'	All	Euro 1	0.0%	43.5%
				X'	All	Euro 2	14.0%	12.5%
				X'	All	Euro 3	33.5%	28.1%
				X'	All	Euro 4	44.2%	15.9%
				X'	All	Euro 5	8.3%	0.0%

Table S7. Evaluation of meteorological parameters simulated by the WRF model over 2013-2017.

	Year	Sample Number	R	Mean Observation	Mean Simulation	MB	RMSE	NMB	NME
Temperature (°C)	2013	5276640	0.97	14.29	13.70	-0.58	3.18	-4.09	16.40
	2014	5247435	0.97	14.30	13.83	-0.47	3.20	-3.32	16.43
	2015	5153973	0.97	14.89	14.34	-0.55	3.16	-3.71	15.56
	2016	5283508	0.97	15.23	14.70	-0.53	3.20	-3.46	15.30
	2017	5368277	0.97	15.12	14.67	-0.45	3.17	-2.95	15.28
Relative humidity (%)	2013	5267041	0.71	69.12	71.34	2.22	15.69	3.21	17.37
	2014	5235871	0.71	68.72	69.98	1.25	15.98	1.82	17.69
	2015	5145148	0.72	69.96	70.95	0.98	15.48	1.41	16.79
	2016	5273974	0.71	70.65	71.36	0.71	15.56	1.01	16.70
	2017	5359708	0.72	69.40	70.04	0.64	15.55	0.93	16.99
Wind speed (m/s)	2013	5151856	0.59	2.73	3.36	0.63	2.13	23.16	59.83
	2014	4996504	0.59	2.74	3.31	0.56	2.09	20.53	57.75
	2015	4924354	0.59	2.76	3.29	0.53	2.07	19.16	57.00
	2016	5066029	0.57	2.71	3.24	0.53	2.07	19.43	58.03
	2017	5178511	0.58	2.71	3.29	0.58	2.10	21.30	58.63
Wind direction (°)*	2013	4406535	0.39	194.34	192.64	4.84	68.01	2.49	25.74
	2014	4287222	0.36	195.67	188.94	4.63	70.25	2.37	26.61
	2015	4165012	0.37	193.57	186.06	5.29	69.17	2.73	26.42
	2016	4242508	0.37	193.45	186.34	4.98	69.22	2.57	26.47
	2017	4340632	0.37	197.33	191.97	4.75	69.19	2.41	25.90
Precipitation (mm)	2013	219040	0.39	5.46	6.40	0.94	14.99	17.20	123.63
	2014	206847	0.38	5.49	6.46	0.97	15.14	17.68	124.69
	2015	229923	0.41	5.58	5.91	0.33	14.44	5.97	115.10
	2016	234745	0.37	6.02	6.35	0.33	15.63	5.51	118.28
	2017	236566	0.39	5.79	6.38	0.60	15.26	10.30	119.31

Note: Units for Mean Observation, Mean Simulation, MB (Mean Bias), RMSE (Root Mean Squared Error) are shown below name of each parameter in the first column, and units for NMB (Normalized Mean Bias), and NME (Normalized Mean Error) are %.

*Mean bias of wind direction is calculated with the consideration of the periodic nature of wind direction. For example, the difference between 1° and 359° is 2° instead of 358°.

References

1. Zheng B*, et al.* (2018) Trends in China's anthropogenic emissions since 2010 as the consequence of clean air actions. *Atmos. Chem. Phys.* 18(19):14095-14111.

2. Zheng B*, et al.* (2015) Heterogeneous chemistry: a mechanism missing in current models to explain secondary inorganic aerosol formation during the January 2013 haze episode in North China. *Atmos. Chem. Phys.* 15(4):2031-2049.

3. Bey I*, et al.* (2001) Global modeling of tropospheric chemistry with assimilated meteorology: Model description and evaluation. *J. Geophys. Res.* 106(D19):23073-23095.

4. Tsinghua University (2016), The MEIC model, Multi-resolution Emission Inventory of China website. Available at: http://www.meicmodel.org/ [Accessed Aug 21, 2018]

5. Li M*, et al.* (2017a) MIX: a mosaic Asian anthropogenic emission inventory under the international collaboration framework of the MICS-Asia and HTAP. *Atmos. Chem. Phys.* 17(2):935-963.

6. Guenther AB*, et al.* (2012) The Model of Emissions of Gases and Aerosols from Nature version 2.1 (MEGAN2.1): an extended and updated framework for modeling biogenic emissions. *Geosci. Model Dev.* 5(6):1471-1492.

7. Gong SL (2003) A parameterization of sea-salt aerosol source function for sub- and super-micron particles. *Global Biogeochem. Cycles* 17(4):1097.

8. Young J. (2012) CMAQv5.0 Windblown Dust, CMAQv5.0 Windblown Dust Website. Available at: https://www.airqualitymodeling.org/index.php/CMAQv5.0_Windblown_Dust [Accessed Aug 21, 2019]

9. Emery C, Tai E, & Yarwood G (2001) Enhanced Meteorological Modeling and Performance Evaluation for Two Texas Ozone Episodes. in *Final Report* (ENVIRON International Corporation).

10. Shen L, Mickley LJ, & Murray LT (2017) Influence of 2000-2050 climate change on particulate matter in the United States: results from a new statistical model. *Atmos. Chem. Phys.* 17(6):4355-4367.

11. Leung DM*, et al.* (2018) Synoptic meteorological modes of variability for fine particulate matter ($PM_{2.5}$) air quality in major metropolitan regions of China. *Atmos. Chem. Phys.* 18(9):6733-6748.

12. Tai APK*, et al.* (2012) Meteorological modes of variability for fine particulate matter (PM2.5) air quality in the United States: implications for $PM_{2.5}$ sensitivity to climate change. *Atmos. Chem. Phys.* 12(6):3131-3145.

13. Cai W, Li K, Liao H, Wang H, & Wu L (2017) Weather conditions conducive to Beijing severe haze more frequent under climate change. *Nat. Clim. Chang.* 7:257.

14. Li M*, et al.* (2017b) Anthropogenic emission inventories in China: a review. *Natl. Sci. Rev.* 4(6):834-866.

15. Zheng B*, et al.* (2017) Resolution dependence of uncertainties in gridded emission inventories: a case study in Hebei, China. *Atmos. Chem. Phys.* 17(2):921-933.

16. Wang X, Dickinson RE, Su L, Zhou C, & Wang K (2018a) $PM_{2.5}$ Pollution in China and How It Has Been Exacerbated by Terrain and Meteorological Conditions. *Bull. Amer. Meteor. Soc.* 99(1):105-119.

17. Ministry of Environmental Protection of the People's Republic of China & General Administration of Quality Supervision, Inspection and Quarantine of the People's Republic of China (2011) Emission standard of air pollutants for thermal power plants. (China Environmental Science Press, Beijing).

18. Zheng B*, et al.* (2018) Infrastructure Shapes Differences in the Carbon Intensities of Chinese Cities. *Environ. Sci. & Technol.* 52(10):6032-6041.

19. National Energy Administration (2013) Notice of the State Council on Issuing the Plan for Energy Development During the 12th Five-Year Plan.

20. Ministry of Environmental Protection of the People's Republic of China & General Administration of Quality Supervision, Inspection and Quarantine of the People's Republic of China (2014) Emission standard of air pollutants for boiler. (China Environmental Science Press, Beijing).

21. Ministry of Environmental Protection of the People's Republic of China & General Administration of Quality Supervision, Inspection and Quarantine of the People's Republic of China (2013) Limits and measurement methods for emissions from light-duty vehicles (CHINA 5). (China Environmental Science Press, Beijing).

22. Zheng Y*, et al.* (2017) Air quality improvements and health benefits from China's clean air action since 2013. *Environ. Res. Lett.* 12(11):114020.

23. Liu J, Han Y, Tang X, Zhu J, & Zhu T (2016) Estimating adult mortality attributable to $PM_{2.5}$ exposure in China with assimilated $PM_{2.5}$ concentrations based on a ground monitoring network. *Sci. Total Environ.* 568:1253-1262.

24. Burnett RT*, et al.* (2014) An Integrated Risk Function for Estimating the Global Burden of Disease Attributable to Ambient Fine Particulate Matter Exposure. *Environ. Health Perspect.* 122(4):397-403.

25. Burnett R*, et al.* (2018) Global estimates of mortality associated with long-term exposure to outdoor fine particulate matter. *Proc. Natl. Acad. Sci. U.S.A.* 115:9592–9597

26. Naghavi M*, et al.* (2017) Global, regional, and national age-sex specific mortality for 264 causes of death, 1980-2016: a systematic analysis for the Global Burden of Disease Study 2016. *The Lancet* 390(10100):1151-1210.

27. Center for International Earth Science Information Network - CIESIN - Columbia University (2016) Gridded Population of the World, Version 4 (GPWv4): Population Count Adjusted to Match 2015 Revision of UN WPP Country Totals. (NASA Socioeconomic Data and Applications Center (SEDAC), Palisades, NY).

28. Jiang X*, et al.* (2015) To what extent can China's near-term air pollution control policy protect air quality and human health? A case study of the Pearl River Delta region. *Environ. Res. Lett.* 10(10):104006.

29. Cohen AJ*, et al.* (2017) Estimates and 25-year trends of the global burden of disease attributable to ambient air pollution: an analysis of data from the Global Burden of Diseases Study 2015. *The Lancet* 389:1907–1918.

30. Zhang D, *et al*. (2015a) Characteristics of $PM_{2.5}$ and its chemical composition in the urban area of Beijing. *Res. of Environ. Sci.* 28(8):1186-1192 (in Chinese).

31. Ding M, *et al.* (2017) Pollution characteristics of NH^{+}, NO_2^{-}, SO_4^{2-} in $PM_{2.5}$ and their precursor Gases During 2015 in an Urban Area of Beijing. *Env. Sci.* 38(4): 1307-1316 (in Chinese).

32. Ji D*, et al.* (2016) Characteristics of atmospheric organic and elemental carbon aerosols in urban Beijing, China. *Atmos. Environ.* 125:293-306.

33. Yang H, Chen J, Wen J, Tian H, & Liu X (2016) Composition and sources of $PM_{2.5}$ around the heating periods of 2013 and 2014 in Beijing: Implications for efficient mitigation measures. *Atmo. Environ.* 124:378-386.

34. Tao J*, et al.* (2015) Aerosol chemical composition and light scattering during a winter season in Beijing. *Atmo. Environ.* 110:36-44.

35. Lin Y-C*, et al.* (2016) Wintertime haze deterioration in Beijing by industrial pollution deduced from trace metal fingerprints and enhanced health risk by heavy metals. *Environ. Pollut.* 208:284-293.

36. Huang R-J*, et al.* (2014) High secondary aerosol contribution to particulate pollution during haze events in China. *Nature* 514:218.

37. Wang Y*, et al.* (2019) Trends in particulate matter and its chemical compositions in China from 2013–2017. *Sci. China. Earth. Sci*. 62: 1857–1871.

38. Wang J*, et al.* (2016a) Characterization and source apportionment of size-segregated atmospheric particulate matter collected at ground level and from the urban canopy in Tianjin. *Environ. Pollut.* 219:982-992.

39. Tao J*, et al.* (2016) Chemical and optical characteristics of atmospheric aerosols in Beijing during the Asia-Pacific Economic Cooperation China 2014. *Atmos. Environ.* 144:8-16.

40. Wei Z*, et al.* (2014) The 2013 severe haze over the Southern Hebei, China: $PM_{2.5}$ composition and source apportionment. *Atmos. Pollut. Res.* 5(4):759-768.

41. Zhang X*, et al.* (2012) Atmospheric aerosol compositions in China: spatial/temporal variability, chemical signature, regional haze distribution and comparisons with global aerosols. *Atmos. Chem. Phys.* 12(2):779-799.

42. Zhang Q, *et al.* (2019) The effects of fine particulate matter constituents on exhaled nitric oxide and DNA methylation in the arginase–nitric oxide synthase pathway. *Environ. Int.* 131:105019.

43. Niu Y, *et al.* (2018) Fine particulate matter constituents and stress hormones in the hypothalamus–pituitary–adrenal axis. *Environ. Int.* 119:186-192.

44. Ming L*, et al.* (2017) $PM_{2.5}$ in the Yangtze River Delta, China: Chemical compositions, seasonal variations, and regional pollution events. *Environ. Pollut.* 223:200-212.

45. Chang Y*, et al.* (2017) Assessment of carbonaceous aerosols in Shanghai, China – Part 1: long-term evolution, seasonal variations, and meteorological effects. *Atmos. Chem. Phys.* 17(16):9945-9964.

46. Ding A*, et al.* (2019) Significant reduction of $PM_{2.5}$ in eastern China due to regional-scale emission control: Evidences from the SORPES station, 2011-2018. *Atmos. Chem. Phys. Discuss.* 2019:1-21.

47. Cao J*, et al.* (2005) Characterization and source apportionment of atmospheric organic and elemental carbon during fall and winter of 2003 in Xi'an, China. *Atmos. Chem. Phys.* 5(11):3127-3137.

48. Tao J*, et al.* (2017) Source apportionment of $PM_{2.5}$ at urban and suburban areas of the Pearl River Delta region, south China - With emphasis on ship emissions. *Sci. Total Environ.* 574:1559-1570.

49. Cui H*, et al.* (2015) Source apportionment of $PM_{2.5}$ in Guangzhou combining observation data analysis and chemical transport model simulation. *Atmos. Environ.* 116:262-271.

50. Wang J*, et al.* (2015) Characteristics and major sources of carbonaceous aerosols in $PM_{2.5}$ from Sanya, China. *Sci. Total Environ.* 530-531:110-119.

51. Liu B*, et al.* (2017) Source apportionment and a novel approach of estimating regional contributions to ambient $PM_{2.5}$ in Haikou, China. *Environ. Pollut.* 223:334-345.

52. Wang J*, et al.* (2016b) Secondary $PM_{2.5}$ in Zhengzhou, China: Chemical Species Based on Three Years of Observations. *Aerosol and Air Qual. Res.* 16(1):91-104.

53. Wang Q*, et al.* (2017) Carbonaceous species in $PM_{2.5}$ and PM_{10} in urban area of Zhengzhou in China: Seasonal variations and source apportionment. *Atmos. Res.* 191:1-11.

54. Feng J*, et al.* (2016) Chemical composition and source apportionment of PM2.5 during Chinese Spring Festival at Xinxiang, a heavily polluted city in North China: Fireworks and health risks. *Atmos. Res.* 182:176-188.

55. Li J*, et al.* (2014) Chemical characteristics and source apportionment of $PM_{2.5}$ during the harvest season in eastern China's agricultural regions. *Atmos. Environ.* 92:442-448.

56. Wang H*, et al.* (2018b) Seasonal characteristics, formation mechanisms and source origins of $PM_{2.5}$ in two megacities in Sichuan Basin, China. *Atmos. Chem. Phys.* 18(2):865-881.

57. Zhang L*, et al.* (2015b) Characteristics of Carbonaceous Species in $PM_{2.5}$ in Wanzhou in the Hinterland of the Three Gorges Reservior of Northeast Chongqing, China. *Atmosphere* 6(4):534-546.

58. Tan J*, et al.* (2016) Chemical characterization of humic-like substances (HULIS) in $PM_{2.5}$ in Lanzhou, China. *Sci. Total Environ.* 573:1481-1490.